1997

Multifrequency eddy current signal analysis

Avanindra
Iowa State University

Multifrequency eddy current signal analysis

by

Avanindra

A thesis submitted to the graduate faculty

in partial fulfillment of the requirements for the degree of

MASTER OF SCIENCE

Major: Electrical Engineering

Major Professor: Satish Udpa

Iowa State University

Ames, Iowa

1997

Graduate College
Iowa State University

This is to certify that the Master's thesis of

Avanindra

has met the thesis requirements of Iowa State University

Signatures have been redacted for privacy

TABLE OF CONTENTS

ACKNOWLEDGEMENTS

I wish to express my most sincere gratitude to my advisor Dr. Satish Udpa for his guidance and invaluable help for this research. His insight and knowledge has motivated me throughout my graduate study. The professional example set by him will always be a source of inspiration. I would also like to thank Dr. Lalita Udpa for her willingness to help whenever I needed to use the MIZ-40 eddy current instrument. I wish to thank my committee members Dr. William Lord, Dr. Greg R. Luecke, Dr. Julie Dickerson and Dr. Lalita Udpa for their support and encouragement. I am also thankful to Kiran Kumar Dasoju and Pradeep Ramuhalli for their help in preparing the slides for my oral examination. I would like to thank all the members of MCRG group at Iowa State University who made working here an enjoyable experience.

I am grateful to my parents, family members and friends for their constant support and encouragement. I wish to dedicate this work to them.

ABSTRACT

This thesis presents a novel procedure for representing and processing multifrequency eddy current signals. Multifrequency eddy current NDE methods are used extensively for the inspection of steam generator tubes in nuclear power plants. Existing methods utilize computationally expensive time domain procedures to process the data. The procedure outlined in the thesis uses frequency domain methods to minimize the computational effort significantly. Two different approaches are evaluated. The first method uses the Fourier descriptor to represent the signal. The Fourier coefficients are utilized to obtain the rotation, scaling and translation parameters required for mixing. The second approach uses the cosine transform. The mixing parameters are derived from the transform coefficients. Fast algorithms can be used to compute the transform. A spin-off of the approach is the ability to obtain rotation, translation and scale invariant parameters from the coefficients directly. Experimental results supporting the validity of the approach are presented.

1 INTRODUCTION

Nondestructive Evaluation (NDE) by definition involves the evaluation of a test specimen for defects without affecting its usefulness or serviceability. Nondestructive evaluation is used widely in various industries for the characterization of materials and the detection of flaws. This is due to the high cost and time requirements associated with destructive methods of testing. Indeed, in many situations destructive testing is not even possible such as in the case of civil infrastructure. In recent years, with advancements in computer technology, a lot of emphasis has been placed on NDE techniques for quality control and maintenance testing, to increase the reliability of manufactured products. NDE also plays a crucial role in areas such as nuclear power and transportation industries in ensuring the integrity of operational components. Safety and a desire for avoiding disruption in service are prime considerations in these cases.

Over the years a multitude of NDE methods have been developed as a result of increased research efforts. These methods address a variety of needs and applications. Prominent among them are ultrasonic, radiographic and electromagnetic methods [15]. Nondestructive evaluation methods share a common strategy. An excitation energy is applied to the test specimen. The interaction between the specimen and the applied energy produces a response signal which contains useful information about the material characteristics or defects. This information is extracted by employing proper signal processing techniques and interpreting the response signal. Computers are used for signal processing and interpretation as well as the storage of the response signal.

Eddy current NDE methods rely on the principles of electromagnetic induction, to

identify or differentiate between a wide variety of physical, structural and metallurgical conditions in electrically conductive materials. Eddy currents offer high sensitivity to surface breaking defects as well as other anomalies that are close to the surface of the specimen. Also eddy current testing techniques are "contactless" and do not require any coupling to the test specimen as is the case with ultrasonic methods.

1.1 Motivation

Eddy current testing is used extensively for testing heat exchanger tubes. A heat exchanger is a device that is used to transfer heat from a fluid flowing on one side of a barrier to another fluid flowing on the other side of the barrier [5]. Heat exchangers are used in a variety of industries, including, power stations, petrochemical plants, oil refineries and air conditioning and refrigeration units. The barrier between the fluids is usually a metal wall such as that of a tube or pipe. Heat exchangers typically utilize a bundle of tubes through which one of the fluids flows. The other fluid is directed in its flow in the space outside the tubes through various arrangements of passes. This fluid is contained by the heat exchanger shell. The most common materials used for tubes is carbon steel and alloy steel because of the strength they offer. Because of excellent heat conductance, different types of brass and copper alloys also find wide use in exchanger manufacture. Corrosion plays a key role in the selection of construction materials. Where corrosion is likely to be a major problem, more expensive corrosion resistant materials such as stainless steels, nickel alloys and titanium may be used. Nuclear power plants, for example use heat exchangers called steam generators that employ Inconel tubes.

Steam generator transfers heat from hot pressurized water in the tubes to the surrounding water which boils and produces steam. The tubing is the boundary between the radioactive water from the reactor, and the steam generated outside, which is used to run turbines. Typically these U-tubes are made from Inconel and are approximately

7.5 m high with an internal diameter of 15.5 mm and 1 mm wall thickness [2]. The array of tubes is forced through holes in the ferromagnetic support plates, which are distributed along their length [19]. The tubing usually becomes radioactive with use making the inspection environment hostile to humans.

Historically steam generator inspection has been a difficult problem. There are numerous examples of unscheduled plant shutdowns. Since a plant outage in a utility can typically cost $500,000 a day, there are strong economic incentives to develop reliable NDE methods. Visual examination and ultrasonic techniques have limited use as they are very slow and only a small percentage of the tubes can be inspected.

These problems have led to a widespread use of eddy current techniques for the inspection of non-ferrous tubing, particularly in the nuclear power industry. In such cases, eddy current inspection offers the following advantages:

- Relatively fast (0.5-1.0 m/s testing speed).
- Can be carried out from inside the tube.
- Can detect both internal and external defects.
- Can detect both gradual and sharp defects.
- Provides quantitative flaw measurements (size, depth etc.).
- Repeatable.
- Lends itself to automated results analysis.
- Can be used to inspect a wide range of tubes.

Disadvantages of eddy current testing are that defects under known support structures (such as support plates,tube sheets, antivibration bars, roll transitions etc.) are

difficult to detect. Figure 1.1 shows some of the support structures that appear as "discontinuities" to the eddy current probe. To examine the issue further, consider a typical situation in a steam generator, some 3600 tubes have to be examined. There are around 10 support plates and a tube sheet anchoring a single tube. Since a nuclear power plant employs four steam generators, this results in over 158,000 sites where there is a high probability that damage in the form of dents, cracks and corrosion pits is present. When the defects are close to support structures the eddy current signal is masked by the response from these structures making it difficult to characterize the defect. The detection of such flaws is critical since failure to identify tubes with flaws in advanced stages of deterioration can lead to catastrophic failure. Proper inspection can help determine which tubes are likely to deteriorate unacceptably before the next overhaul. Such tubes may then be plugged or replaced, depending on the condition of the steam generator. In addition to the detection of such defects, eddy current testing can also be used to monitor other conditions, such as build up of external sludge and to verify the degree of expansion at tube sheets during manufacture [3].

One method of overcoming the difficulty of isolating the defect signal from the artifact signals is to collect eddy current data at more than one excitation frequency. When data at many frequencies are available, it is possible to eliminate the effect of unwanted variables. In general, at least as many independent eddy current readings must be taken as there are properties whose variation may affect the readings [28]. If sinusoidal eddy currents are used, only two independent quantities, such as the magnitude and phase, can be measured at each frequency. Therefore, if more than two properties need to be determined, multiple frequencies should be used. The increased amount of information gained using multifrequency methods, may be combined to nullify unwanted signal components.

This thesis presents some new techniques for processing multifrequency data to eliminate unwanted signals. Examples of unwanted signals include support plates, dents and

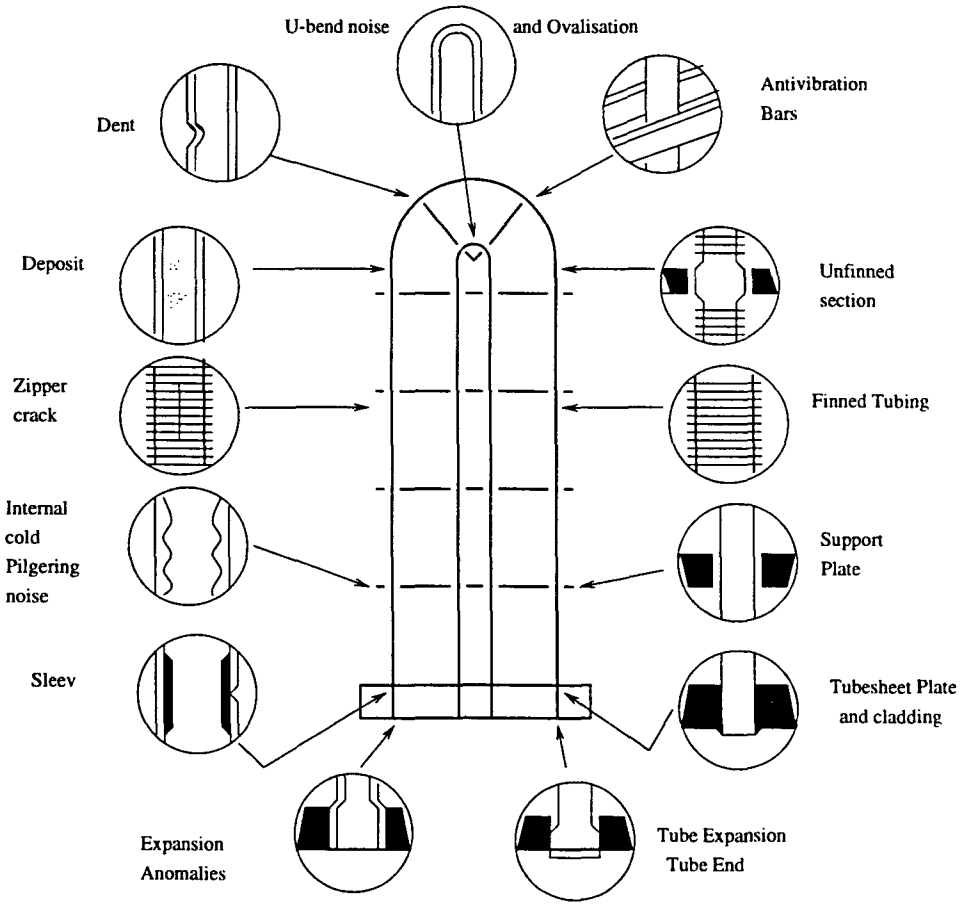

Figure 1.1 Heat Exchanger Design and Manufacturing Discontinuities [14]

magnetite deposits on the outside of tubes. These benign signals sometimes mask harmful defect signals. Multifrequency processing techniques can be employed to suppress the unwanted signals without degrading the quality of defect signals. Other desirable features that are sought also include low computational complexity in order to ensure that the algorithm can be implemented in real time.

Both time and frequency domain approaches for processing the multifrequency data are evaluated. The time domain method eliminates the unwanted signal by minimizing a cost function in the least squares sense. A drawback is that the method is computationally intensive. The problem is minimized by employing fast algorithms and taking advantage of the underlying heuristics. This allows the approach to be implemented in

real time.

1.2 Summary of contributions and outline of thesis

This thesis explores the feasibility of using frequency domain approaches for reducing the computational burden. Methods that are evaluated include Fourier series and discrete cosine transform based approaches where the frequency domain coefficients of the signals containing information are used for suppressing the benign signals. The desirable feature of frequency domain techniques is that they require a fixed amount of computation. This makes these approaches superior to the time domain techniques. The validity of the approach is established using simulated as well as experimental data.

An additional outcome of the research is that cosine transform based features that are insensitive to rotation, scaling and translation of the original signal can be obtained. The invariant features offer a benefit in that the features allow independent scaling of the real and imaginary components of the eddy current signal. These invariant descriptors can be used for the classification of defect signals in automated nondestructive evaluation systems.

Chapter 2 presents an introduction to the principles of eddy current nondestructive evaluation. Both single and multifrequency eddy current methods are described. A brief description of various multifrequency analysis systems that are currently used in industry is also included.

A new approach for analyzing multifrequency eddy current signals is presented in chapter 3. The chapter describes novel time and frequency domain techniques developed for processing multifrequency eddy current signals. A section is devoted to describe the cosine transform based features that are invariant to signal rotation, scaling and translation.

Chapter 4 discusses the results obtained by applying the multifrequency techniques

to suppress support plate signals. The results are compared with those obtained using a commercially available multifrequency instrument. This is followed by a section that presents a few concluding remarks and recommendations for future work.

2 PRINCIPLES OF NONDESTRUCTIVE EDDY CURRENT EVALUATION

2.1 Basics of single frequency eddy current testing

When a coil carrying an alternating current is brought in close proximity to a material, an electromotive force proportional to the rate of change of the magnetic field is induced in accordance with Faraday's law of electromagnetic induction. If the material is conducting, closed current loops are established in the material. These are called eddy currents. In conformity with Lenz's law, the direction of the induced eddy currents, and consequently the secondary field generated by these currents, is such as to oppose the change in the primary field [6]. This is shown in Figure 2.1.

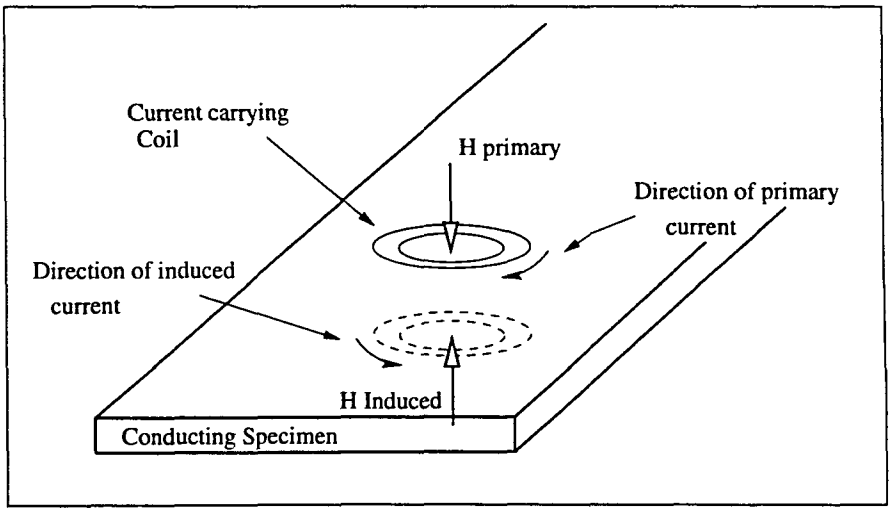

Figure 2.1 Alternating current coil over a conducting specimen showing direction of primary and induced current

Assuming that the specimen is nonferromagnetic, the flux linkages associated with the coil decreases because of the opposing nature of the primary and secondary fields. The inductance of the coil, which is defined as the flux linkage per ampere, consequently decreases as the coil is brought close to the specimen [30]. Accompanying the decrease in inductance is an increase in resistance, to account for the eddy current losses in the specimen. The presence of discontinuity or inhomogeneity in the test specimen causes a reduction as well as a redistribution of the eddy currents as shown in the Figure 2.2. Consequently, the changes in the coil impedance are reduced.

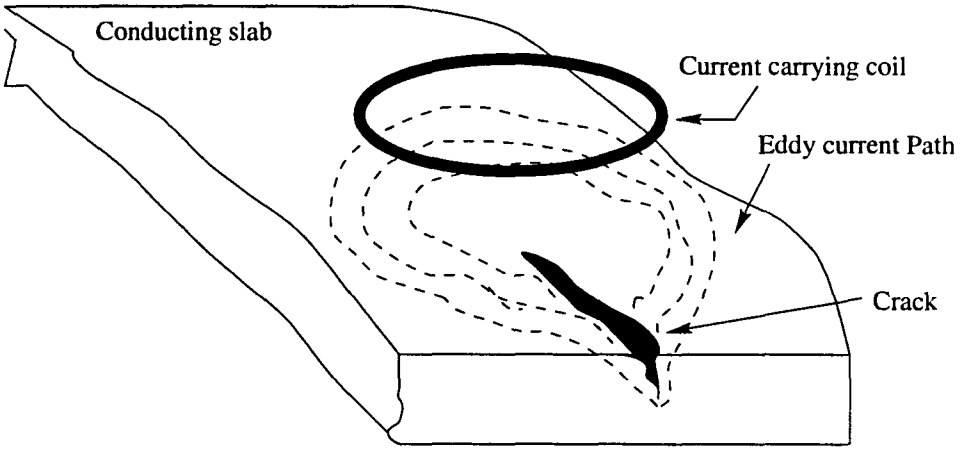

Figure 2.2 The disturbance of the flow of eddy current in the material due to the presence of a defect

Eddy current responses of a single coil may be conveniently described by reference to the "impedance plane". This is a graphical representation of the complex probe impedance where the abscissa (X value) represents the resistance and the ordinate (Y value) represents the inductive reactance [10]. Figure 2.3 shows the change in impedance for a nonferromagnetic conducting specimen under different conditions. The underlying process is more complicated when the test specimen is ferromagnetic. Due to the higher permeability of the material the inductance of the coil increases [6]. This effect, very often, dominates the decrease in inductance due to eddy currents. The resistance

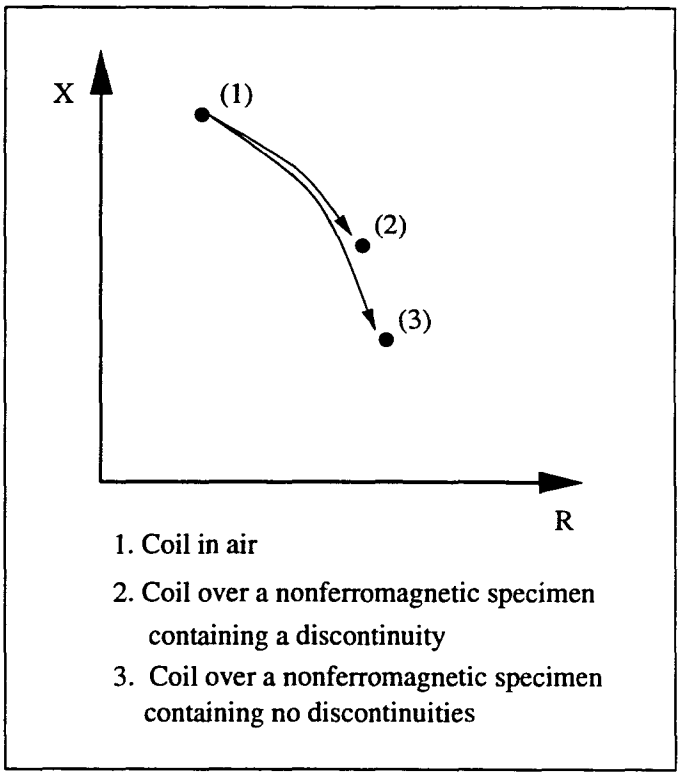

Figure 2.3 Impedance plane trajectory of a coil over a nonferromagnetic specimen with and without a discontinuity; changes are greatly exaggerated for clarity

also increases due to eddy current and hysteresis losses.

The variations in coil impedance caused by discontinuities in the test specimen are often very small in comparison with the quiescent value of the coil impedance. The detection and measurement of these small changes is often accomplished using bridge circuits [17]. Factors which influence the eddy current field, [16] [5] and therefore the coil impedance, are:

- the separation between the coil and surface, called lift-off.
- the electrical conductivity of the specimen.
- the magnetic permeability of the specimen.

- the frequency of the AC inducing the eddy current field.
- the design of the eddy current probe
- geometric factors,
- discontinuities such as cracks, corrosion, pitting.

Successful detection and characterization of flaws requires a careful design of signal processing procedures to negate or compensate for these effects. It is this elimination of undesired response that forms the basis of much of the technology of eddy current inspection. The following paragraphs explain the effect of each of the factors.

As mentioned earlier, lift-off is the separation or distance between the probe and specimen surface. The closer a probe coil is to the surface the greater will be the effect on coil impedance. This has two main effects: The "lift-off" signal is generated as the probe is moved on and off the surface and there is a reduction in sensitivity as the coil to material spacing increases. This fact is used to design probes to give a better response signal as described in the next section.

The conductivity of test specimen has a very direct effect on the eddy current flow: the greater the conductivity of the test material, the greater the flow of eddy currents on the surface. Conductivity is often measured by an eddy current technique. Based on the conductivity measurement inferences can be drawn about the different factors which affect conductivity, such as material composition, heat treatment, surface coating thickness, etc.

The magnetic permeability of a material may be described as the ease with which a material can be magnetized. For non-ferrous metals such as copper, brass etc., and for austenitic stainless steels the permeability is the same as that of 'free space'. For ferrous metals however, the relative permeability μ_r may be several hundred, and this has a very

significant influence on the eddy current response. In addition the permeability varies greatly within a metal part due to localized stresses and heating effects.

Geometric factors such as finite dimensions, curvature, edges, grooves etc. affect the eddy current distribution and hence the response also. Test techniques must recognize this, for example to test for a crack near an edge, the probe should be moved parallel to the edge so that any change in response is due to a discontinuity and not due to the fact that eddy current redistributes near an edge. The effect of frequency and probe configuration are also factors which affect eddy current response. These are factors which can be controlled by the designer. These are explained in greater detail in the following sections.

The change in the impedance of the coil, which is known as the eddy current signal is measured by most instruments. The amplitude and phase of the signals can be displayed on a cathode ray oscilloscope. Impedance plane diagrams are also used for displaying eddy current signals. The analysis of these signals and interpretation give information about a variety of material properties including conductivity, permeability, specimen thickness and lift-off. In the case of tube inspection, the phase of the signal can give important information regarding the nature of the defect and depth.

2.1.1 Eddy current probes

One obvious factor which influences the impedance of the coil is its configuration. It is necessary to use a coil which is most sensitive to the kind of defects expected during the test. Hence the choice of probes is dictated by the specimen to be evaluated. Several different probe types are available. Sometimes special probes are designed to meet the needs of a specific application. The probe configurations described below are for inspecting tubes.

An absolute probe which is a single coil wound circumferentially, is sensitive to both inner diameter (ID) and outer diameter (OD) defects [7]. As the name suggests, an

absolute probe can be used to evaluate conditions in absolute terms. It is useful for measuring conditions which change slowly along the tube, such as gradual metal loss (thinning). However due to sensitivity to slowly changing conditions, it is often difficult to accurately identify smaller defects. In addition, changes in the coil parameters. due to environmental factors and lift-off, can often mask changes due to discontinuities, making signal interpretation very difficult. Figure 2.4 shows absolute mode response for different defects.

A variation of the absolute eddy current probe is the differential eddy current probe. Figure 2.5 shows a differential eddy current probe designed for inspecting tubes and the response signal to various defects. The probe consists of two identical coils mounted on the same axis as the tube but spaced apart by a small distance. The two coils form the two arms of a bridge circuit. The bridge imbalance signal is the voltage difference across the impedance of the two coils. As the probe is scanned past a discontinuity, the change in impedance of the leading coil when it scans a discontinuity results in an imbalance voltage. The differential voltage traces a trajectory b1-a2-b2 in the impedance plane as shown in Figure 2.5. Similarly when the trailing coil scans the discontinuity, the differential impedance traces the trajectory b2-c2-b3 in the opposite direction. The shape of the impedance plane trajectory is a function of the nature of the discontinuity. Figure 2.5 shows the eddy current signals for different types of defects.

Differential probes give extremely accurate evaluation of small defects such as internal pitting. Using a differential test, it is possible to evaluate both the size and depth of defects, so that a small hole can be distinguished from a large area of shallow pitting. Some other probes that are used are cross axis and driver-pickup probes [7] [14]. A cross axis probe is a special type of differential probe in which one coil is wound circumferentially, as in a standard coil, with the second coil in line with the tube. The second coil is sensitive to circumferential cracks, to which a standard differential coil gives very little response.

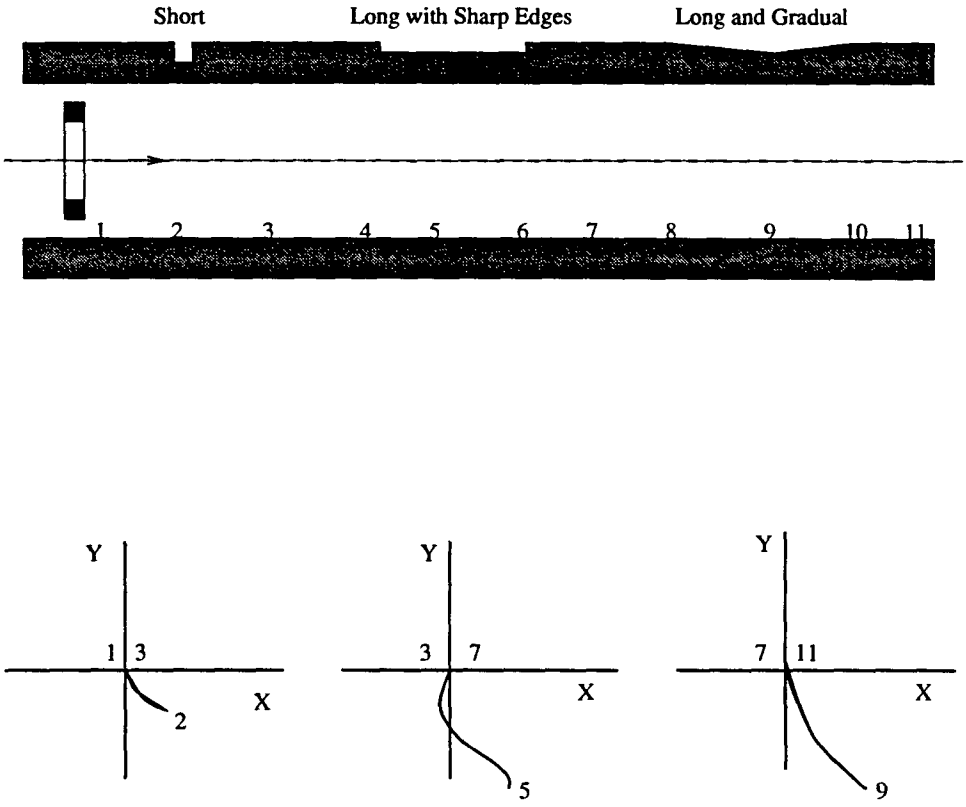

Figure 2.4 Absolute mode response to discontinuities in a tube [14]

Driver-pickup coils have three coils. A driver coil is connected to the oscillator circuit of the instrument, and the resulting magnetic field is sensed by separate pickup coils. This has the advantage that the coil characteristics can be better optimized for the job they are to perform. A comparison of Figures 2.5 and 2.4 demonstrates the sensitivity of absolute and differential probes to gradual and sharp defects respectively.

Ocassionally a combination of absolute and differential coils is used for complete defect characterization. For the eddy current test to be sensitive, the probe should fit the tube as closely as possible. If the probe is a sloppy fit there will be two problems [7]. There is excessive noise due to wobble or lift-off, which makes it difficult to measure signal phase, hence the defect cannot be characterized. Secondly the sensitivity is reduced: particularly to defects at one end of the tube, due to the probe lying on the diametrically

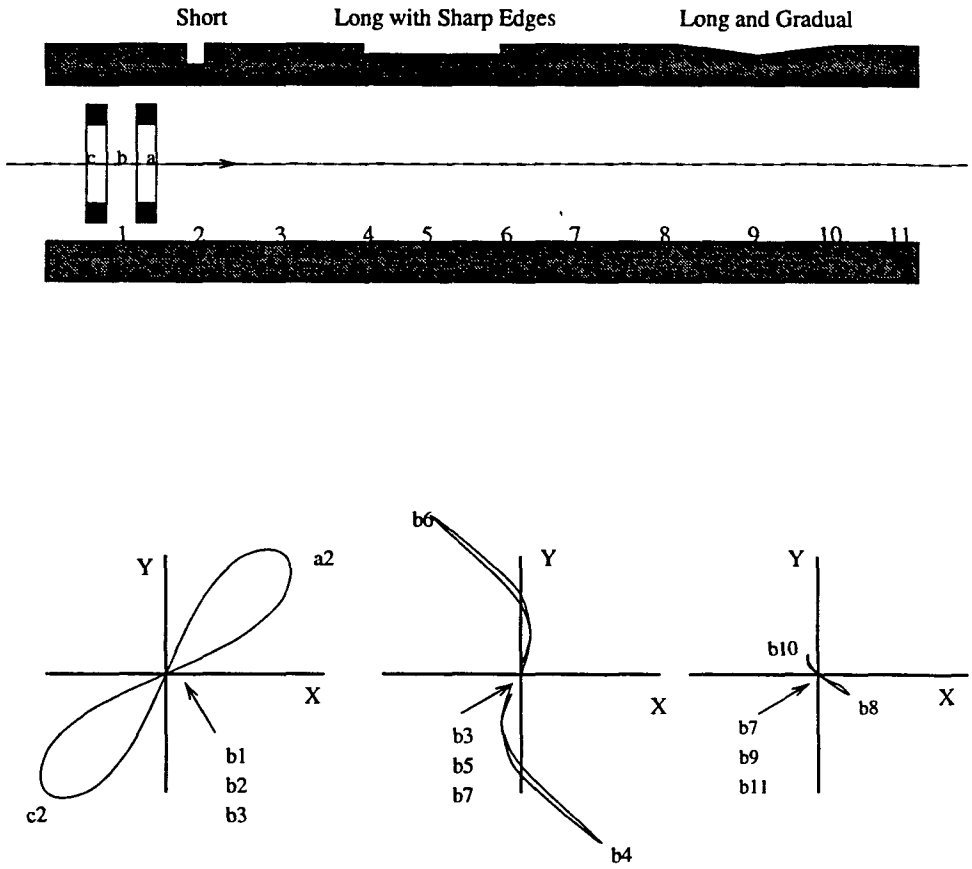

Figure 2.5 Differential mode response to discontinuities in a tube [14]

opposite end. If the probe is too tight, there is risk of it sticking in the tube, especially when there are dents in the tube. Therefore it is necessary to allow some clearance. The 'goodness of fit' is commonly expressed in terms of fill-factor - the ratio of probe cross-sectional area to tube ID squared. Usually a fill factor of 0.7 or more is considered a good fit.

2.1.2 Frequency selection

The selection of probe excitation frequency is the primary eddy current test parameter under operator control. Frequency selection affects both the magnitude of response from different flaws and the phase relationship. Thus selection of operating frequency

is very important in obtaining good resolution of flaw signals in the presence of other variables which may affect the test. The frequency selected for an eddy current test is influenced by several factors. The frequency selected should be sensitive to all the flaws and should be able to accurately size them. It should be sensitive to all relevant extraneous discontinuities, and should be able to discriminate them from the damage. An important criterion that is used in frequency selection is the "depth of penetration". The eddy current density, and thus the strength of the response from a flaw, is greatest on the surface of the material being tested [13] and declines in some special cases exponentially with depth as shown in Figure 2.6. Hence higher frequencies enable inspection of areas near or on the surface of the metal whereas lower frequencies allow inspection of defects that are deeper within the specimen. The excitation frequency of the eddy current probe is typically between 10 Hz and 10 MHz [18].

The "standard depth of penetration or skin depth" δ is defined by the formula:

$$\delta = \frac{1}{\sqrt{\pi \mu \sigma f}} \tag{2.1}$$

where

f is the excitation frequency,

μ is the magnetic permeability,

σ is the electrical conductivity

This is the depth at which the eddy current is $1/e$ (37%) of its surface value when an infinite half sheet of current is induced in a metallic half plane. In the case of tube inspection the skin depth merely serves as a useful measure to consider in choosing the excitation frequency for a given material (μ and σ).

The frequency selected is thus influenced by the tubing wall thickness and conductivity of the material. Thicker walls require a lower frequency so that all the defects

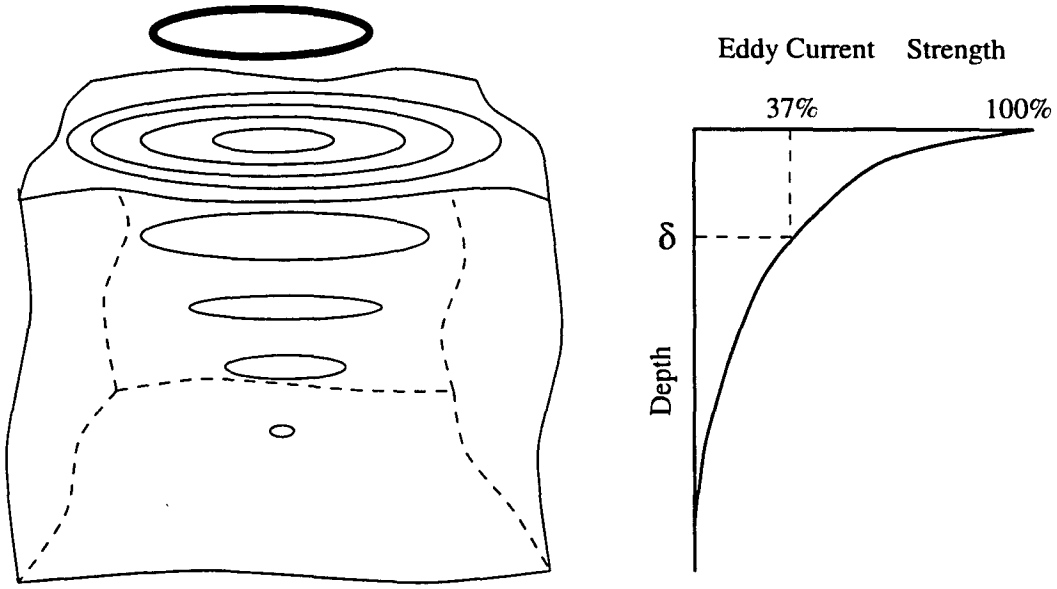

Figure 2.6 Depth of penetration for an infinite conductive half space

within the tube can be characterized. Other factors being equal, the frequency chosen is inversely proportional to the material conductivity, since higher the conductivity lower is the depth of penetration. The frequency selected is also dictated by the required form of response; most commonly a test is set up in accordance with a specification such as ASME boiler and pressure vessel code. For differential testing this means that the probe wobble signal is set horizontally on the screen and the displayed phase of a through wall hole is approximately 45 degrees clockwise from the horizontal [7] . The final selection of the frequency is done using an appropriate calibration tube.

In order to provide accurate defect analysis, it is necessary to obtain a piece of tube of the same material and dimensions as the tubes to be inspected and use it for calibration of the instrument. Defects similar to those that are likely to occur during inspection, are introduced into this specimen piece. These defects have known size and origin and can be used for calibration. This is essential to optimize the frequency and sensitivity setting required in order that actual defects can be classified relative to the reference defects. Some calibration tubes attempt to simulate the types of defects encountered in service

[5]. For example, flat bottomed holes can be used to simulate pitting corrosion, spark eroded notches can be used to simulate cracks and machined circumferential grooves can be used to simulate general thinning. The main advantage is that more accurate depth assessment of defects can be given.

As an aside, for ferromagnetic material the relative permeability is typically 500-2000 [5]. This means that for ferromagnetic materials the eddy currents are concentrated on the surface and defects that are buried deep in the tube wall are not detectable. Also, small variations in permeability gives rise to relatively high noise levels. Hence eddy current inspection techniques have limited applicability to ferromagnetic tubing inspection.

2.2 Multifrequency eddy current techniques

2.2.1 Need for multifrequency testing

Single frequency eddy current tests offer excellent sensitivity to a number of different types of steam generator tubing under normal conditions. However conditions are often complicated by a number of factors and consequently inspection needs cannot be effectively solved by single frequency examination. Some extraneous discontinuities (such as tube support plate, internal noise due to sludge build up, probe wobble, dents etc.) distort or mask defect signals which are located near them [4]. This creates mistaken interpretation of the eddy current signal resulting in unnecessary tube plugging. Lack of detection may also lead to unexpected leaks and costly shutdowns. The detection of other discontinuities such as wall thinning, sludge height, dents etc. needs several successive probe passes at different frequencies and measurement mode [23]. This increases the inspection time, which from safety as well as economic reasons should be kept to a minimum.

State of the art multifrequency eddy current testing overcomes most of the single

frequency limitations. The multifrequency technique consists of collecting data simultaneously using several excitation frequencies from just one probe pulling. This provides data which are analyzed using multifrequency mixing or multiparameter techniques. This technique allows the effect of extraneous discontinuities to be "nullfied". Alternating currents of different frequencies are either summed and sent simultaneously to the test coil, or multiplexed and sent successively. After frequency separation, using bandpass filters or the timing information in multiplexed method, the coil impedance is estimated and displayed for each frequency separately. Multiparameter or mixing techniques are then used to analyze the data to classify and characterize the defects. Several superimposed test frequencies are sent to the probe. The frequency which would be used normally when conducting a single frequency examination is the basic frequency or primary frequency. The others are auxiliary frequencies. As the probe passes under a discontinuity, the signatures obtained using different excitation frequencies can be compared.

As mentioned earlier, each frequency is sensitive to a certain type of discontinuity. A typical inspection uses three or four frequencies in both differential and absolute modes. Low frequencies have a large skin depth and hence give clear signals from support structures which are located away from the coil. They are sometimes used to determine location along the tube. They can also be used to detect loose parts on the outside of the tubes such as magnetite deposits. High frequencies have a much smaller skin depth and for defects on the outside of the tube, the depth can be estimated from the phase of the eddy current signal [2] [5]. Higher excitation frequency also gives information about the probe wobble when the fill factor of the probe is low. Because of the different skin depths at different frequencies, the relationship between signals from defects and support features changes with frequency. Consequently, it is possible to combine the signals from two different frequencies so as to subtract out a support feature but leave the signal from defect. In effect, this means that multifrequency response signals have more information

which can be analyzed to extract relevant features. Thus multifrequency techniques have the following advantages [14]:

- Collects data at several test frequencies simultaneously. This decreases inspection time by preventing retesting of the tube with another frequency.
- Decreases the in-service inspection time and human exposure to radiation in nuclear plant inspections.
- Allows separation of discontinuities which give similar signals at one frequency.
- Improves sensitivity to different types of discontinuities.
- Easy interpretation of complex signals.
- Improves the detection, interpretation and sizing of defects even in the presence of artifacts that complicate the analysis procedure.
- Can also be used in conjunction with multimode (differential or absolute) technique for complete analysis.

2.2.2 Fundamentals of multifrequency eddy current inspection

The multifrequency method is useful for solving multiple signal problems, i.e. when the useful defect signal occurs with background noise or in the presence of a benign signal from a support structure. The basic assumption, confirmed by practice, is the linear superposition of the signals which states "the signal resulting from two discontinuities, or from one discontinuity and background noise, is equal to the linear combination (vectorial sum) of two signals considered separately". The whole concept of multifrequency analysis is based on this important "linearity principle". Figure 2.7 and 2.8 show the result of adding different discontinuities in a tube, from a differential probe. In Figure 2.7 both the external and the internal defects are less than 10% of the tube wall

thickness. The presence of the two defects at the same location, leads to the resultant signal which has a phase similar to a through hole defect signal. Note that in Figure 2.7 if the defect signatures are associated with vectors as shown, the resultant signal can be interpreted as vector addition of the ID and OD defect signals. This interpretation is possible since the two defect signals have similar shape. For Figure 2.8 also, the principles of vector operation apply, but since the two signals have completely different shapes it is not as apparent. The assumption of linearity is valid under very restrictive conditions [28], A more detailed discussion of issue as well as methods for nonlinear combination of signals have been proposed by Horne et al. [8] and others [27].

The multifrequency analysis uses a composite signal and subtracts the undesirable signal to leave only the useful defect signal, as if the useful signal had been detected alone. Thus the problem is to produce the signal used for subtraction.

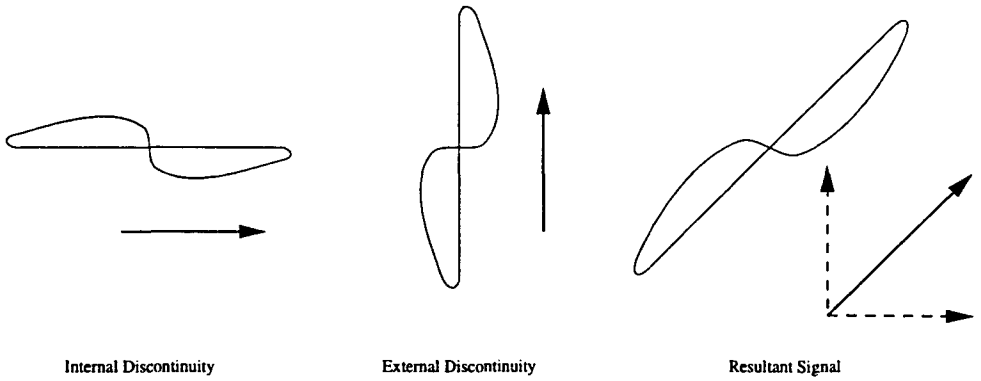

Figure 2.7 Impedance plane trajectories observed when using a differential probe on internal and external discontinuities in a tube along with their vectorial representation

The result of subtraction would be perfect if the undesirable signal alone were available. The signal can then be directly subtracted from the composite signal to obtain the defect signature. This is sometimes possible, when the signal is perfectly repeatable each time an inspection is carried out. In such cases there is no need for using multiple excitation frequencies. However, the multifrequency process is far more flexible

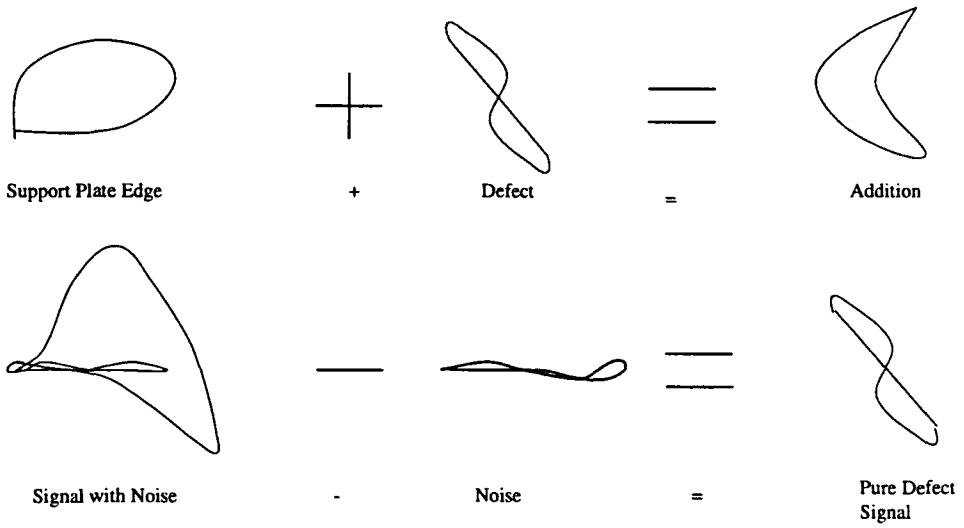

Figure 2.8 Demonstration of linearity principle

and versatile because the signal need not be stored; it simply has to be measured at more than one frequency. The measurement is done using the same probe excited with multiple frequencies, with the auxiliary excitation frequency selected such that it results in a preferential detection of the signal to be eliminated. Unfortunately the test carried out at the auxiliary frequency is sensitive to both the undesirable signal and the defect signal. Subtraction of auxiliary signal from the primary frequency signal does not cancel the extraneous discontinuity signal; changing the frequency also changes the sensitivity and the nature of the response to discontinuities. The net effect is that the desired signal is also altered in amplitude and the phase is changed. Thus the signal interpretation procedure has to be adjusted to account for these factors. Figure 2.9 explains this phenomenon in terms of vectors.

The auxiliary or mixing frequency is chosen such that the amplitude and phase separation between the defect and the unwanted discontinuity signals is very different from that obtained at the basic excitation frequency. Also the mixing frequency should not be too different, otherwise the signal shapes would not be retained, which is required for mixing. In reality when two undesirable responses to the two frequencies are adjusted in

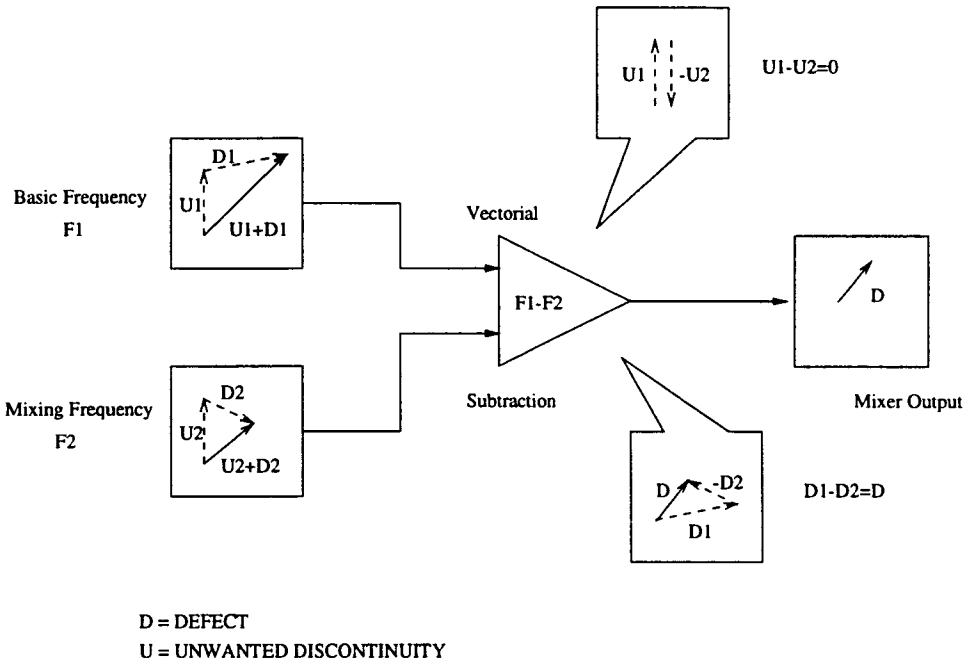

Figure 2.9 Two frequency mix principle to suppress one unwanted discontinuity [14]

amplitude and phase, their waveforms are slightly different, resulting in a residual. The aim is to minimize this residual which looks like noise in the defect signal after mixing. With the gain and phase controls of the mixing frequency, the unwanted discontinuity (U2) signal is shaped in phase and amplitude to match its basic frequency signal (U1). Then subtraction in the mixer eliminates the unwanted signal. Before subtraction, the defect signal has a different amplitude and phase at the basic (D1) and mixing (D2) frequencies; subtraction does not cause suppression of the defect signal. The resulting defect (D) signal is displayed at the mixer output. This is treated as response of a system that is sensitive to defects, but insensitive to the suppressed unwanted discontinuity.

A significant advantage of mixing is that it is purely static; the result of the signal combination is absolutely independent of the probe movement speed so that the result is the same at rest, at low or high speed [17].

2.2.3 Operating principles of multiparameter analysis systems

Multifrequency eddy current testing uses the amplitude and phase parameters at different frequencies to separate the discontinuity signals. These parameters vary differently under different frequencies and hence when data is collected at more than one frequency, there is enough information to isolate the effect of extraneous or benign discontinuities. Manufacturing and design discontinuities are referred to as benign signals. Various analysis systems are used for suppression of a given parameter. These systems have signal outputs from two channels corresponding to the test frequencies $f1$ and $f2$. The signals represent the inphase and quadrature components of the complex impedance of the probe. For test frequency $f1$, let the inphase or real component be $x1$ and imaginary component be $y1$. Similarly for test frequency $f2$, let the real and imaginary components be $x2$ and $y2$. The signal processing methods that are commonly used are the algebraic method, coordinate transform method and phasor rotation and subtraction or combinations of these method [27]. Each of these methods are described next.

2.2.3.1 Algebraic method

The algebraic method assumes that the multifrequency data are linear functions of n parameters. These parameters represent n discontinuities or changes such as conductivity, permeability, support plates, wall thickness or defects present in the specimen. This assumption is valid if there is a linear relationship between variations in the parameters and the probe impedance. It has been verified experimentally and shown to be valid under small signal conditions [12] [13]. The component values a_{ij} and P_j are measured from some zero, null or nominal values. This is also consistent with the general practice adopted by commercial eddy current test equipment where the output signals represent deviations from some input null, reference or electrical bridge balance conditions.

In the case of a two frequency system, the signals are expressed as follows:

$$\begin{aligned} x_1 &= a_{11}P_1 + a_{12}P_2 + a_{13}P_3 + a_{14}P_4 \\ y_1 &= a_{21}P_1 + a_{22}P_2 + a_{23}P_3 + a_{24}P_4 \\ x_2 &= a_{31}P_1 + a_{32}P_2 + a_{33}P_3 + a_{34}P_4 \\ y_2 &= a_{41}P_1 + a_{42}P_2 + a_{43}P_3 + a_{44}P_4 \end{aligned} \tag{2.2}$$

where

P_1, P_2, P_3 and P_4 are the parameters

and a_{ij} is the coefficient of parameter P_j

The solution of these equations is given by

$$\begin{aligned} P_1 &= c_{11}x_1 + c_{12}y_1 + c_{13}x_2 + c_{14}y_2 \\ P_2 &= c_{21}x_1 + c_{22}y_1 + c_{23}x_2 + c_{24}y_2 \\ P_3 &= c_{31}x_1 + c_{32}y_1 + c_{33}x_2 + c_{34}y_2 \\ P_4 &= c_{41}x_1 + c_{42}y_1 + c_{43}x_2 + c_{44}y_2 \end{aligned} \tag{2.3}$$

Coefficient c_{ij} may be obtained either by calculation after the signals have been digitized or by the successive approximation method. This is done in the calibration stage where typical values of parameter P_j are measured using standards appropriate for the kind of specimen to be evaluated.

Figure 2.10 shows the basic system for a two frequency instrument, which directly outputs the desired parameter. Additional circuits are needed for more parameters.

A variation of the algebraic method is used by Prince et. al. for the measurement of Zircaloy cladding thickness on uranium [24]. Slightly enriched uranium is extruded into a tubular shape and coated with zircaloy. As part of the quality assurance program,

the fuel elements must be 100 percent surface inspected for zircaloy clad thickness. It is observed that the cladding thickness bears an exponential relation with the signal amplitude and can, therefore be estimated using a polynomial of the form:

$$\begin{aligned} t &= b_1 + b_2 \ln V_{50k} + b_3 \ln V_{5M} + b_4 (\ln V_{50k})^2 + \\ & \quad b_5 (\ln V_{5M})^2 + b_6 (\ln V_{50k})(\ln V_{5M}) \end{aligned} \tag{2.4}$$

where

t is the clad thickness

$b_1 \cdots b_6$ are coefficients

V_{50k} and V_{5M} are signal amplitudes at 50 kHz and 5 MHz respectively.

Two different frequencies are used to remove the effect of lift-off variations. The 5 MHz signal is sensitive to lift-off and 50 kHz signal is sensitive to both lift-off and clad thickness. The coefficients are calculated using fuel element clad thickness standards at different lift-off and thickness conditions. The data obtained is fitted to the above polynomial by minimizing the square error. The authors obtain an accuracy of 0.025 mm for the clad thickness with the lift-off varying from 0.102 to 0.305 mm.

2.2.3.2 Coordinate transformation method

This method also defines a set of parameters. It is assumed that each parameter is represented by a vector in a space of n dimensions. The curves displayed on the instrument represent the evolution of the end of these vectors on a projection plane corresponding to the frequency used. If the test frequency is changed, the projection plane rotates around its own axis, thus modifying the phase shift between the discontinuity signals [17].

The method suppresses the effects of undesired artifacts by applying successive rotation and projection transforms to the probe coil impedance data. The discrimination is

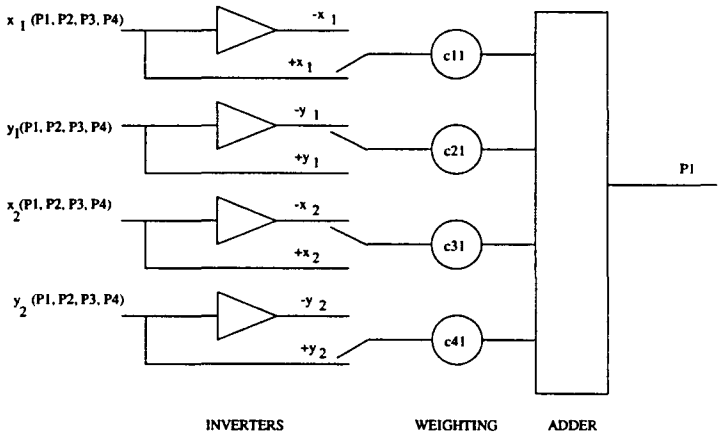

Figure 2.10 Analog multiparameter system using algebraic method for parameter P1 [17]

achieved by projecting the undesired data on to a hyperplane and the defect data on to a plane which is normal to the hyperplane. For a two frequency instrument, there are two projection planes corresponding to each frequency. As shown in Figure 2.11 using various components one of the planes is rotated within the space and a plane is reconstituted so that only parameter $P4$ has a vertical component and the other parameters coincide with the horizontal axis.

The complex impedance plane data can be rotated by applying the two dimensional coordinate transformation.

$$\begin{aligned} x' &= x\cos\phi + y\sin\phi \\ y' &= -x\sin\phi + y\cos\phi \end{aligned} \tag{2.5}$$

where

x and y are the initial coordinates of the signal

x' and y' are the coordinates obtained after rotation ϕ

The goal of successive rotations is to transform the unwanted parameters onto one plane. Figure 2.12 shows how this is achieved for a two frequency instrument. Each

rotator is a ganged sine-cosine potentiometer and is configured as shown. When the signals are available as digital data, the rotation transformations may be carried out using a digital signal processor. The three phase shifters, which are identical and can rotate the input signal from $0 - 360$ degrees independent of each other, are connected in cascade. The phase shifters are adjusted until the desired parameter is normal to the unwanted ones. The four parameters $P1, P2, P3, P4$ are shown in Figure 2.11(a). The phase shifters ϕ_1 and ϕ_2 are adjusted successively to obtain the separation of the required parameter $P1$ (shown in Figure 2.11(b) and 2.11(c)). Parameters $P2, P3$ and $P4$ coincide in 2.11(e). Phase shifter ϕ_3 adjusts the residual signals $P2, P3$ and $P4$ horizontally so that only the parameter $P1$ has a vertical component. The resulting signal is displayed on an oscilloscope. The separation of parameters needs a careful choice of frequencies [26].

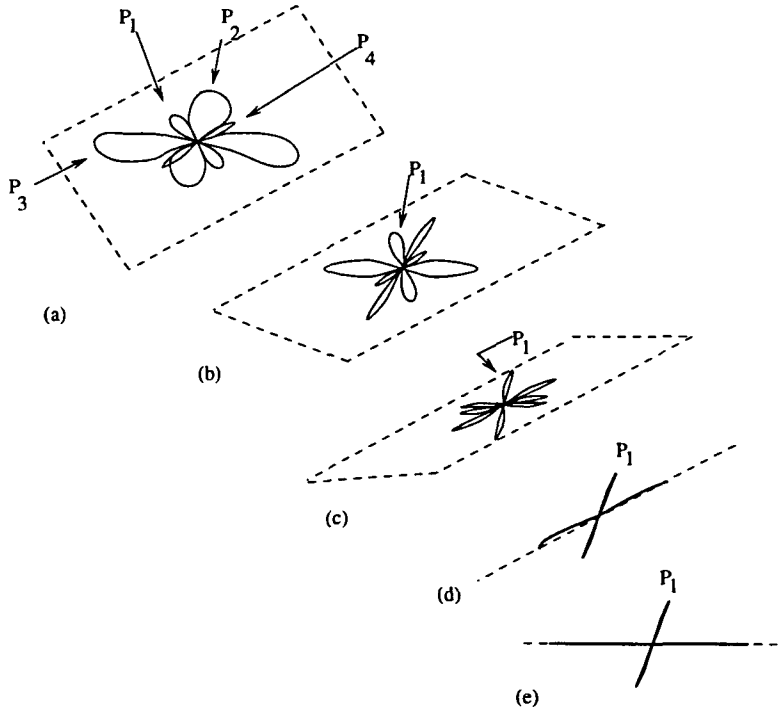

Figure 2.11 Adjustment steps for coordinate transformation [17]

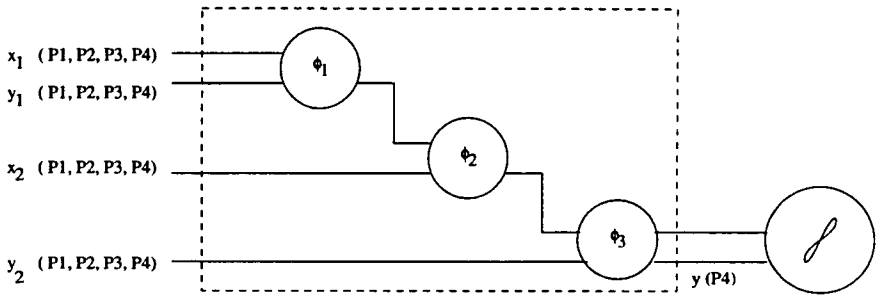

Figure 2.12 General coordinate transformation system

2.2.3.3 Combination method

This is one of the more commonly used methods. One frequency is used for elimination of each parameter although it might sometimes be possible to eliminate more than one parameter using the auxiliary frequency. The primary frequency is chosen such that it is more sensitive to the defect while the auxiliary frequencies are used to remove the effect of benign artifacts or noise as explained in detail earlier.

Figure 2.13 shows various stages in parameter elimination. It is assumed that only two parameters exist. $P1$ is the parameter to be eliminated and $P2$ is the discontinuity signal. The continuous curve represents the signals obtained using the primary excitation frequency and the dashed curve represents the signals corresponding to the auxiliary frequency.

Processing involves (1) modifying the curve $P1'$ by weighting to make it similar to $P1$ as shown ($P1''$ in Figure 2.13(b)). (2) executing a phase rotation to superimpose the signal $P1''$ and $P1$. (3) subtracting the components of the signals [17] as follows :

$$x_1 - x_1'' \qquad (2.6)$$

$$y_1 - y_1''$$

This is the same as vectorial subtraction explained earlier. The components of the disturbing signal $P1$ are canceled out, while the discontinuity signal components retain

a significant value.

The system can be extended for mixing and eliminating more than one parameter. For example, to simultaneously eliminate the effect of support plate as well as dent another auxiliary frequency is added. The auxiliary frequency f_1 is sensitive to the support plate while f_2 is sensitive to dents. The combination of f_1 and f_2 with the basic excitation frequency signal removes the effect of the support plate. The combination of the signals thus obtained further removes the effect of the dent, so that the final mix shows only the defect signal.

An alternate approach requires only two mixers. Mixing f_1 and the basic frequency signal gives an output with partial subtraction of support plate. This signal is mixed with f_3 to completely suppress the support plate and dent. Both methods need two auxiliary frequencies. These have been tested extensively in the field. The results obtained from both methods are same although the two mixer method is more difficult to optimize. However it has the advantage that it is less operator dependent than the three mixer method. The three mixer method has the advantage that three mixing outputs are available for analysis. These mixers can be optimized to suppress various combinations of extraneous discontinuities such as: support plate and dent, expansion transition and tube sheet plate, internal pilgering noise and support plate, antivibration bar and U-bend transition, probe wobble and copper deposits, and so on.

The next chapter presents some novel algorithms that have been developed for mixing the basic and auxiliary frequency signals efficiently. These algorithms implement steps (1) and (2) of the combination method.

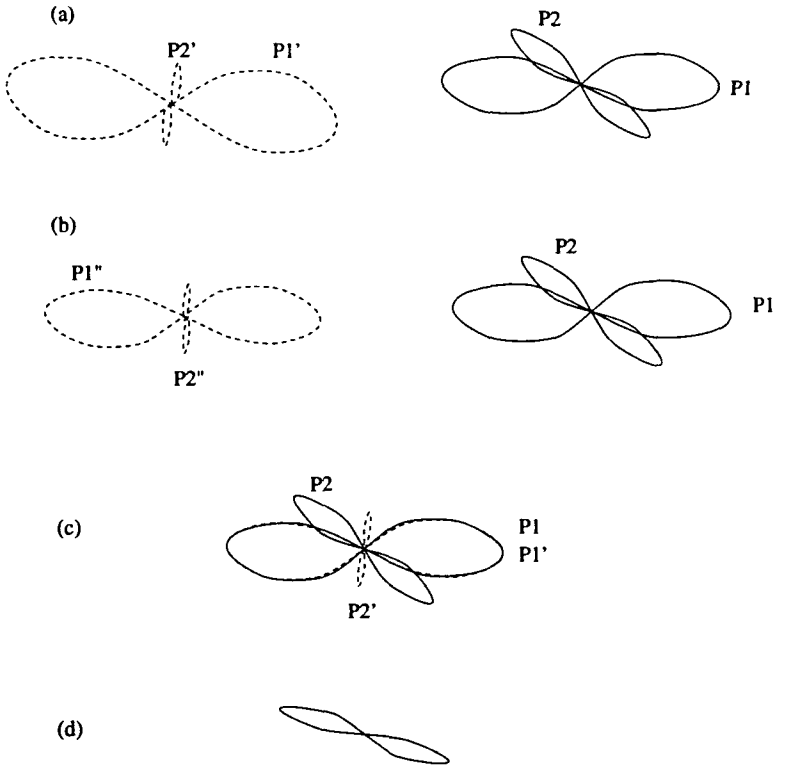

Figure 2.13 Adjustment stages in the combination method: (a) signals before analysis; (b) signals after weighting; (c)signals after phase rotation; and (d) signals after subtraction

3 ALGORITHMS FOR MULTIPARAMETER SIGNAL ANALYSIS

3.1 Introduction

The objective of a mixing algorithm is to subtract the undesirable signal component generated by an artifact from a composite signal to produce the defect signal. This is accomplished by conducting the eddy current test at two excitation frequencies. The first excitation frequency is chosen so as to ensure the highest level of sensitivity to the artifact. The auxiliary frequency data is then rotated, translated and scaled such that it resembles the composite signal. The transformed auxiliary signal is subtracted from the composite signal to obtain the defect signal. The purpose of the procedures presented in this chapter is to shape and rotate the auxiliary frequency signals appropriately. The success of the multiparameter method is dependent on the efficiency with which the transformation procedure is implemented. Extensive survey of the available literature showed a lack of such methods. Most systems use a calibration stage in which the mixing parameters (the weights for shaping the signal and the rotation angle) are calculated off-line. These parameters are then used to transform the auxiliary frequency signal for subtraction from the basic frequency signal as the probe is scans the tube. This is an inefficient approach, as the mixing parameters are optimized for suppression of a particular kind of discontinuity. In addition it is likely that the nature of the discontinuity being suppressed may differ from the artifact standard used during the calibration stage. Hence the mixing may not be optimum. An alternative approach is to mix signals using

the procedure described earlier. This has the advantage that mixing is optimized for each discontinuity and is not dependent on a reference standard. For such a method to be effective, the mixing algorithms have to be computationally efficient so that the results of mixing can be seen in real time. In this thesis the signals are shaped and rotated using affine transformations [11].

3.2 Affine transformation equations

An affine transformation is employed to rotate, scale and translate an eddy current signal such that it resembles a second eddy current signal [29].

Translation is represented by the following equations.

$$\begin{aligned} x' &= x + T_x \\ y' &= y + T_y \end{aligned} \tag{3.1}$$

or

$$[x'\ y'\ 1] = [x\ y\ 1] \begin{bmatrix} 1 & 0 & 0 \\ 0 & 1 & 0 \\ T_x & T_y & 1 \end{bmatrix} \tag{3.2}$$

where

x, y are the original coordinates of a point in the plane

x', y' are the transformed coordinates

T_x is the X-axis translation

T_y is the Y-axis translation

The operation of rotation in the counter-clockwise direction about the origin is obtained by:

$$x' = x\cos\theta - y\sin\theta$$

$$y' = x \sin\theta + y \cos\theta$$

or

$$[x'\ y'\ 1] = [x\ y\ 1] \begin{bmatrix} \cos\theta & \sin\theta & 0 \\ -\sin\theta & \cos\theta & 0 \\ 0 & 0 & 1 \end{bmatrix} \tag{3.3}$$

where

x, y are the original coordinates of a point in the plane

x', y' are the transformed coordinates.

θ is the angle of rotation

Scaling is achieved by:

$$\begin{aligned} x' &= S_x x \\ y' &= S_y y \end{aligned} \tag{3.4}$$

or

$$[x'\ y'\ 1] = [x\ y\ 1] \begin{bmatrix} 1 & 0 & 0 \\ 0 & 1 & 0 \\ S_x & S_y & 1 \end{bmatrix} \tag{3.5}$$

where

x, y are the original coordinates of a point in the plane

x', y' are the transformed coordinates

S_x is the X-axis scaling coefficient

S_y is the Y-axis scaling coefficient

Thus the transformations can be combined and written using a compact notation as:

$$[x', y'] = [x, y, 1]\mathbf{A} \tag{3.6}$$

where

$$\mathbf{A} = \begin{bmatrix} S_x \cos\theta & S_y \sin\theta \\ -S_x \sin\theta & S_y \cos\theta \\ S_x(T_x \cos\theta - T_y \sin\theta) & S_y(T_x \sin\theta + T_y \cos\theta \end{bmatrix} \tag{3.7}$$

A is referred to as the affine transform matrix.

The objective of the mixing algorithm is to estimate the parameters T_x, T_y, θ, S_x and S_y such that the transformed auxiliary signal data is as close to the primary signal data as possible.

3.3 Conjugate gradient method

The optimum affine transform parameters can be estimated using a least squares estimation procedure in the time domain [29]. Let S_b be the basic frequency signal and S_a be the auxiliary frequency signal. Then S'_a the transformed signal is given by:

$$S'_a = S_a\mathbf{A}(S_x, S_y, T_x, T_y, \theta)$$

The error function E is defined as the square of the error between the transformed version of the auxiliary frequency data and the primary frequency data.

$$E = ||S_a\mathbf{A} - S_b||^2 \tag{3.8}$$

The optimum values of the affine transform parameters are estimated by minimizing the error function E. This involves solving the following five nonlinear equations simultaneously.

$$\frac{\partial E}{\partial T_x} = 0 \tag{3.9}$$

$$\frac{\partial E}{\partial T_y} = 0 \tag{3.10}$$

$$\frac{\partial E}{\partial \theta} = 0 \tag{3.11}$$

$$\frac{\partial E}{\partial S_x} = 0 \tag{3.12}$$

$$\frac{\partial E}{\partial S_y} = 0 \tag{3.13}$$

Solving this system of equations yields the affine transform parameters, that is optimum in the minimum error squares sense. Each of the sequences S_a and S_b are represented by n samples in the impedance plane. The fully expanded form of these five equations is as follows:

$$\begin{aligned} 2\sum_{i=1}^{n}\{[x_{di} &- (S_x\cos\theta)x_i + (S_x\sin\theta)y_i - S_xT_x\cos\theta \\ &+ S_xT_y\sin\theta][-S_x\cos\theta] + [y_{di} - (S_y\sin\theta)x_i \\ &+ (S_y\cos\theta)y_i - S_yT_x\sin\theta - S_yT_y\cos\theta] \\ &* [-S_y\sin\theta]\} = 0 \end{aligned} \tag{3.14}$$

$$\begin{aligned} 2\sum_{i=1}^{n}\{[x_{di} &- (S_x\cos\theta)x_i + (S_x\sin\theta)y_i - S_xT_x\cos\theta \\ &+ S_xT_y\sin\theta][S_x\sin\theta] + [y_{di} - (S_y\sin\theta)x_i \\ &- (S_y\cos\theta)y_i - S_yT_x\sin\theta - S_yT_y\cos\theta] \\ &* [-S_y\ \cos\theta]\} = 0 \end{aligned} \tag{3.15}$$

$$\begin{aligned} 2\sum_{i=1}^{n}\{[x_{di} &- (S_x\cos\theta)x_i + (S_x\sin\theta)y_i - S_xT_x\cos\theta \\ &+ S_xT_y\sin\theta][(S_x\sin\theta)x_i + (S_x\cos\theta)y_i \\ &+ S_xT_x\sin\theta + S_xT_y\cos\theta] + [y_{di} - (S_y\sin\theta)x_i \\ &- (S_y\cos\theta)y_i - S_yT_x\sin\theta - S_yT_y\cos\theta] \end{aligned}$$

$$
\begin{aligned}
& * \quad [(-S_y \cos\theta)x_i + (S_y \sin\theta)y_i - S_y T_x \cos\theta \\
& + \quad S_y T_y \sin\theta]\} = 0 \qquad (3.16) \\
2\sum_{i=1}^{n}[x_{di} & - \quad (S_x \cos\theta)x_i + (S_x \sin\theta)y_i - S_x T_x \cos\theta \\
& + \quad S_x T_y \sin\theta][(-cos\theta)x_i + (\sin\theta)y_i - T_x \cos\theta \\
& + \quad T_y \sin\theta] = 0 \qquad (3.17) \\
2\sum_{i=1}^{n}[y_{di} & - \quad (S_y \sin\theta)x_i - (S_y \cos\theta)y_i - S_y T_x \sin\theta \\
& - \quad S_y T_y \cos\theta][(-\sin\theta)x_i - (\cos\theta)y_i - T_x \sin\theta \\
& - \quad T_y \cos\theta] = 0 \qquad (3.18)
\end{aligned}
$$

where

x_{di}, y_{di} is the primary frequency data, the elements of sequence S_b

x_i, y_i is the auxiliary frequency data, the elements of sequence S_a

Since the gradient function is available, one of several descent methods can be utilized for minimizing the error E. Many of these are iterative methods and require an initial choice of the parameters. In each successive step, new values of the parameters are generated. The cost function (in this case, the error E) is evaluated for the new parameters and tested for convergence. The iterative procedure is repeated if the convergence criterion is not satisfied, otherwise the current values of the parameters are taken to be optimum. Descent methods that can be employed include the steepest gradient, conjugate gradient or Fletcher-Reeve's method, Newton's method and the variable metric method [25]. The steepest descent method and conjugate gradient method were evaluated since they are intuitively satisfying and allow heuristics to be included to speed up convergence. The Newton and variable metric method require extra storage, and consequently were not evaluated.

The flow chart for Fletcher-Reeve's method is shown in Figure 3.1. The vector $\mathbf{X}_i$

shown in the Figure is defined as:

$$\mathbf{X}_i = \begin{bmatrix} T_{xi} \\ T_{yi} \\ \theta_i \\ S_{xi} \\ S_{yi} \end{bmatrix} \tag{3.19}$$

where

i stands for i^{th} iteration

∇E is the gradient of the error function defined as:

$$\nabla E = \begin{bmatrix} \frac{\partial E}{\partial T_x} \\ \frac{\partial E}{\partial T_y} \\ \frac{\partial E}{\partial \theta} \\ \frac{\partial E}{\partial S_x} \\ \frac{\partial E}{\partial S_y} \end{bmatrix} \tag{3.20}$$

The algorithm starts with an initial estimate of the vector $\mathbf{X}_i$ denoted $\mathbf{X}_1$. The gradient of the cost function E is evaluated at $\mathbf{X}_1$. Vector $\mathbf{S}_i$ is the search direction used to update $\mathbf{X}_i$

$$\mathbf{X}_{i+1} = \mathbf{X}_i + \lambda_i \mathbf{S}_i \tag{3.21}$$

where

λ_i is the step length.

In general at the i^{th} iteration, the vector $\mathbf{S}_i$ is defined as:

$$\mathbf{S}_i = -\nabla E_i + (|\nabla E_i|^2 / |\nabla E_{i-1}|^2)\mathbf{S}_{i-1} \tag{3.22}$$

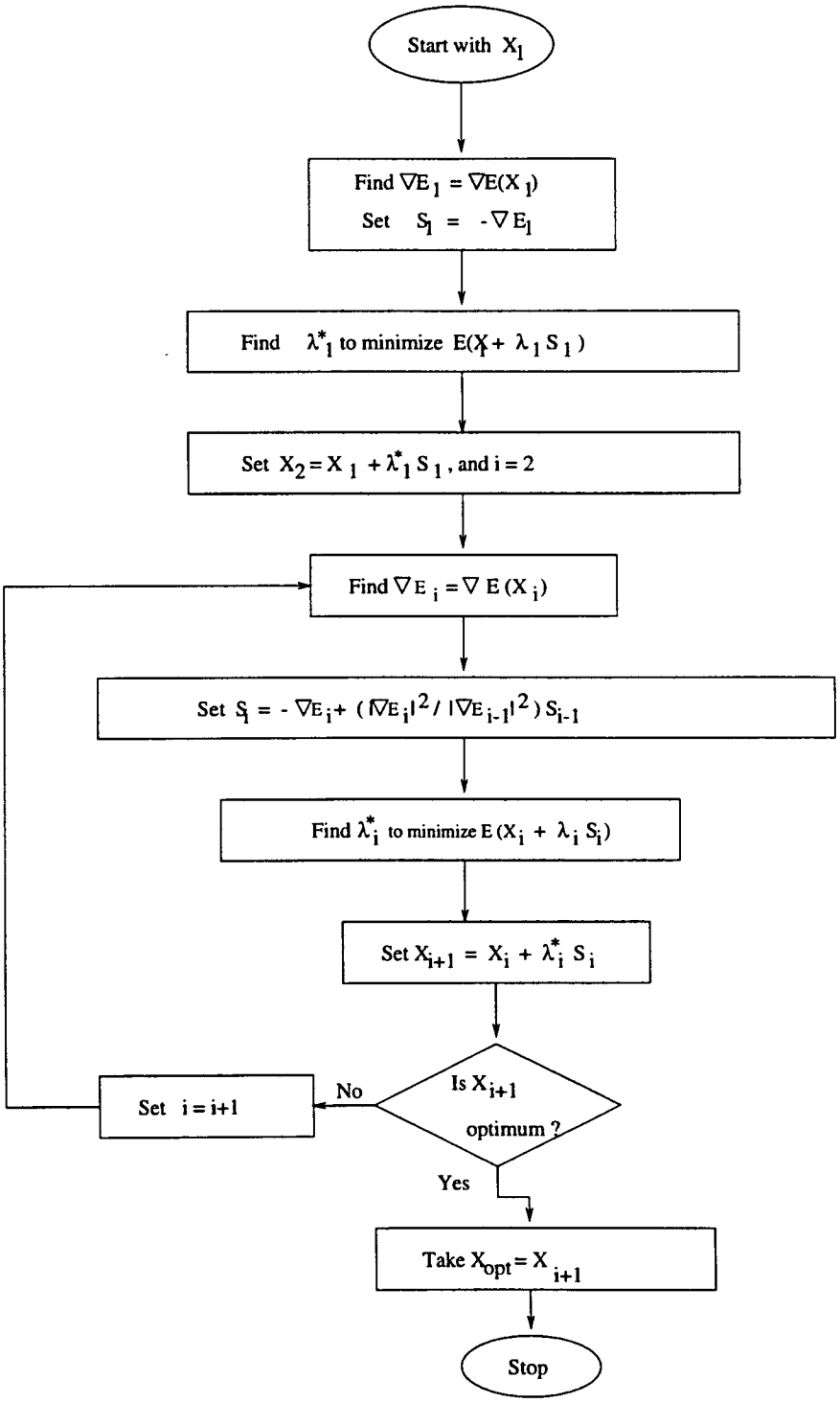

Figure 3.1 Flow chart for the Fletcher-Reeves method

The steepest descent method is a special case of the more general Fletcher-Reeve's method where $\mathbf{S}_i$ is always defined as

$$\mathbf{S}_i = -\nabla E_i$$

It has been suggested for the conjugate gradient method that after every m iterations $\mathbf{S}_i$ should be chosen as

$$\mathbf{S}_i = -\nabla E_i$$

to reduce the cumulative effect of round off errors. In the actual implementation, m was chosen by experimentation to be 5 or 6. This is close to the recommended value [rao] of $m = k + 1$ where k is the number of design variables. For the affine transform minimization case, the number of variables $k = 5$.

The choice of λ to minimize $E(\mathbf{X}_i + \lambda_i \mathbf{S}_i)$ requires another minimization process within each iterative step. A heuristic method, explained later, is used for choosing the optimal value of λ_i. Another step in the flow chart that needs explanation is the choice of convergence criterion. As the gain of the impedance plane data and also the number of samples or data points in the impedance plane is not fixed, an absolute value for the error E cannot be used. Instead the convergence criterion is based on the derivative, i.e.

$$\left|\frac{\partial E}{\partial x_j}\right| \leq \epsilon \qquad \forall\ j = 0, 1, 2, 3, 4 \tag{3.23}$$

where

x_j is the j^{th} component of vector $\mathbf{X}_i$.

This is true, since all the partial derivatives are close to zero when the parameter estimates are close to the optimal value. The value of ϵ is chosen to be 10^{-3}. A lower value only tends to increase the number of iterations without affecting the quality of the parameter estimates significantly.

It was observed that by using the same initial estimates for the parameters, the conjugate gradient method requires fewer iterations to converge than the steepest gradient method. However the quality of the estimates were superior to the steepest descent method.

3.3.1 Heuristics to improve conjugate gradient minimization

The conjugate gradient method can be improved by choosing good initial estimates for the transformation parameters, namely $T_x, T_y, \theta, S_x, S_y$. θ_1 is obtained by setting it equal to the phase difference between the two impedance plane trajectories S_a and S_b. S_{x1} is chosen as the ratio of the inphase phase component of the amplitude of the two signals. Similarly S_{y1} is the ratio of the quadrature components of the amplitude of the signals. T_x and T_y are initially set to a value representing the difference between the averages of the two signals. This significantly reduces the number of iterations. For the example presented in Figure 3.3, the number of iterations is reduced by a factor of ten. The approach has been tested using real data and gives good initial estimates of the parameters. As an example, Figure 3.2 shows a through-hole defect signal in the presence of a support plate at auxiliary excitation frequency, that is translated to match the primary excitation frequency data using the initial estimates of the translation parameters.

A reduction in the computational complexity at each iterative step can be achieved by considering the equations used for calculating the partial derivatives . If the summation is taken inside in equations (3.14) through (3.18), the sum need not be performed for $i = 0$ to $i = n$ at each iterative step. Thus equation (3.14) becomes :

$$\frac{\partial E}{\partial T_x} = -2[\sum_{i=1}^{n} x_{di} - (S_x \cos\theta) \sum_{i=1}^{n} x_i + (S_x \sin\theta)$$

$$
\begin{aligned}
* \quad & \sum_{i=1}^{n} y_i - n * S_x T_x \cos\theta + n * S_x T_y \sin\theta] \\
* \quad & [-S_x \cos\theta] + [\sum_{i=1}^{n} y_{di} - (S_y \sin\theta) \\
* \quad & \sum_{i=1}^{n} x_i + (S_y \cos\theta) \sum_{i=1}^{n} y_i - n * S_y T_x \sin\theta \\
- \quad & n * S_y T_y \cos\theta] * [-S_y \sin\theta]
\end{aligned} \tag{3.24}
$$

If we define the running and product sums as,

$$
\begin{aligned}
X_{di} &= \textstyle\sum_{i=1}^{n} x_{di} & Y_{di} &= \sum_{i=1}^{n} y_{di} \\
X_i &= \textstyle\sum_{i=1}^{n} x_i & Y_i &= \sum_{i=1}^{n} y_i \\
Sum_{xx} &= \textstyle\sum_{i=1}^{n} x_i x_i & Sum_{x_d x_d} &= \sum_{i=1}^{n} x_{di} x_{di} \\
Sum_{yy} &= \textstyle\sum_{i=1}^{n} y_i y_i & Sum_{y_d y_d} &= \sum_{i=1}^{n} y_{di} y_{di} \\
Sum_{xy} &= \textstyle\sum_{i=1}^{n} x_i y_i & Sum_{x_d y_d} &= \sum_{i=1}^{n} x_{di} y_{di} \\
Sum_{x_d x} &= \textstyle\sum_{i=1}^{n} x_{di} x_i & Sum_{y_d y} &= \sum_{i=1}^{n} y_{di} y_i \\
Sum_{x y_d} &= \textstyle\sum_{i=1}^{n} x_i y_{di} & Sum_{x_d y} &= \sum_{i=1}^{n} x_{di} y_i
\end{aligned} \tag{3.25}
$$

the computational effort in calculating ∇E at each iterative step is minimized. Another advantage is that the performance of the algorithm is independent of the sampling rate of the impedance plane data since the number of samples in the impedance plane data does not affect convergence speed. This is evident from the fact that the data is used only once to compute various terms defined in equations (3.25).

The method implemented for estimating the optimum value of the step size λ has a significant effect on the performance of the algorithm due to the fact that it is repeated in each iteration. Various alternatives are available such as choosing a small constant

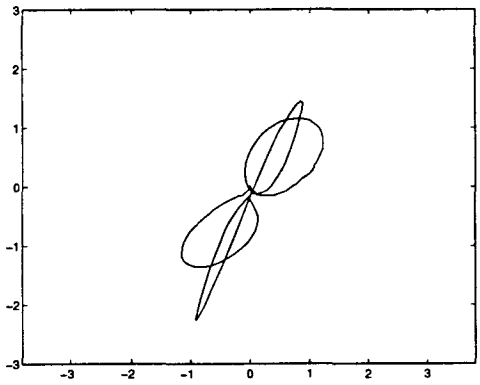

(a) Primary frequency signal at 400 kHz

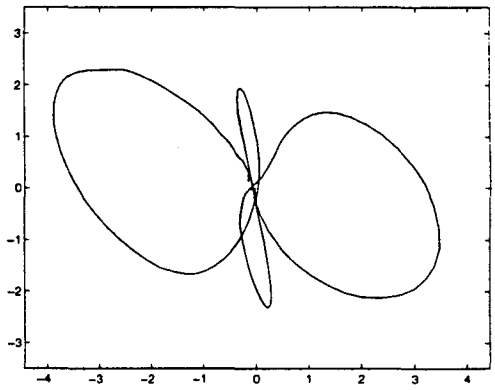

(b) Auxiliary frequency signal at 200 kHz

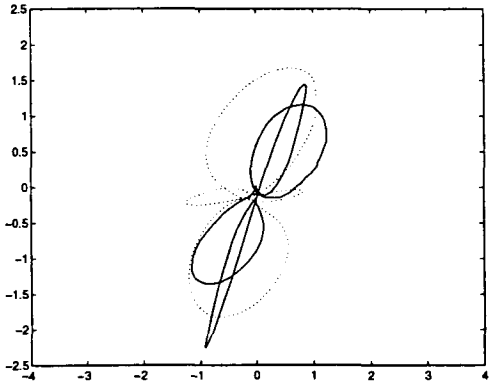

(c) signal in (b) translated to (a)

Figure 3.2 Signal transformation for a through hole defect in the presence of support plate using initial estimates

step size, or using an appropriate optimization technique for minimizing $E(X_i + \lambda_i S_i)$ as a function of λ_i. Different methods were used to choose an optimal value of λ. The drawback associated with choosing constant λ is that it is difficult to select a value which works well under all conditions. An inappropriate value of λ may result in divergence of the iterative procedure. In contrast, a small value of λ results in poor performance. The Newton-Raphson method was used to estimate optimal values of λ. Though Newton-Raphson method reduces the number of iterations, the overall effect is to slow down the algorithm since the method is a computationally intensive procedure.

A heuristic method is used in the final implementation to choose the values of λ at each iterative step. Initially λ is chosen to be a sufficiently small number which ensures that the cost function does not increase. As the iterative procedure progresses, λ is chosen as follows:

IF $E_i^{test} < E_{i-1}$ THEN

$\lambda = \lambda\alpha, \quad \alpha > 1.0$

ELSE

$\lambda = \lambda\beta, \quad 0.0 < \beta < 1.0$

Go back to the beginning of IF statement

The parameters controlling the adaptation of λ are experimentally found to be:

$$\lambda^{start} = 10^{-5}, \qquad \alpha = 1.2 \qquad \text{and} \qquad \beta = 0.9$$

The validity of the approach was evaluated using finite element model (FEM) impedance plane data. The FEM model [21] was used to simulate an inner diameter tube defect at frequencies of 25 kHz and 50 kHz. The impedance plane trajectories obtained using the FEM are presented in Figure 3.3(a) and 3.3(b). The estimated values of the transformation parameters are: $T_x = 0.0805$, $T_y = -0.0486$, $\theta = -155.7377$, $S_x = -2.6682$ and

$S_y = 1.8923$. The auxiliary frequency data was then mapped using these transformation parameters. The results are shown in Figure 3.3(c). As can be seen, the auxiliary frequency data is closely mapped to the primary frequency data. Additional results are presented in the next chapter.

3.4 Fourier series method

The algorithm presented in the last section is based on a time domain approach. Alternatively, the transformation parameters can be estimated using frequency domain methods. The strategy involves estimating the transformation parameters based on information contained in frequency components of the primary and auxiliary impedance plane data. We use the Fourier series expansion of the signals to obtain the frequency domain representation.

Consider a simple closed impedance plane curve in the two dimensional coordinate system as shown in Figure 3.3(a). We obtain a parametric representation of the impedance plane curve by representing each point as a function of the arc length l along the curve, measured from an arbitrary starting point P_0. Thus $(x(l), y(l))$ is a point on the curve located l arc length units away from the starting point. Next we define a function $u(l)$ as:

$$u(l) = x(l) + jy(l), \qquad j = \sqrt{-1} \tag{3.26}$$

If L is the total length of the curve then,

$$u(l + nL) = u(l), \qquad n = \ldots -1, 0, 1, \ldots$$

The periodicity of the function $u(l)$ allows its expansion in a Fourier series. Thus

$$u(l) = \sum_{n=-\infty}^{\infty} c_n \exp\left[\frac{j2\pi nl}{L}\right] \tag{3.27}$$

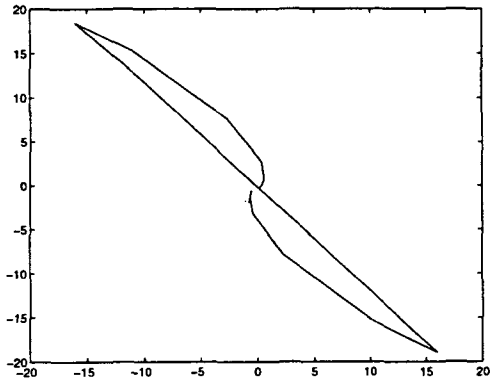

(a) Primary frequency signal at 50kHz

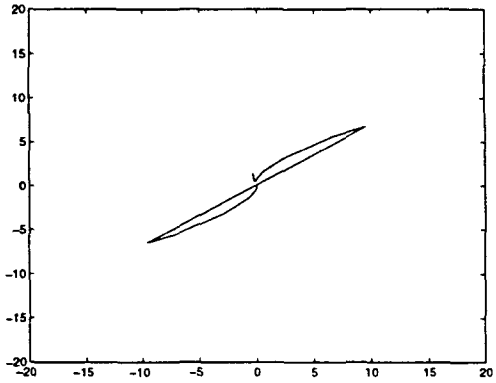

(b) Auxiliary frequency signal at 25kHz

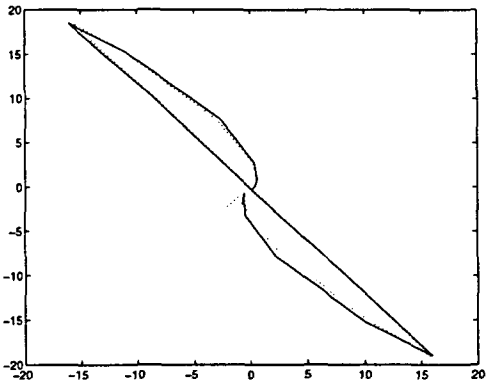

(c) signal in (b) translated to (a)

Figure 3.3 Signal transformation for FEM generated data using the conjugate gradient method

where

$$c_n = \frac{1}{L}\int_0^L u(l)\exp(\frac{-j2\pi nl}{L})dl \tag{3.28}$$

If the curve is translated by T_x and T_y, rotated by θ and scaled by S the Fourier coefficient c'_n of the translated curve is given by [31]:

$$\begin{aligned} c'_n &= \frac{1}{L}\int_0^L Sexp(j\theta)(u(l)+T_x+jT_y)\exp(\frac{-j2\pi nl}{L})dl \\ &= \frac{Sexp(j\theta)}{L}\int_0^L u(l)\exp(\frac{-j2\pi nl}{L})dl \\ &\quad + \frac{Sexp(j\theta)}{L}\int_0^L (T_x+jT_y)\exp(\frac{-j2\pi nl}{L})dl \\ &= \frac{Sexp(j\theta)}{L}\int_0^L u(l)\exp(\frac{-j2\pi nl}{L})dl \qquad n\neq 0 \end{aligned} \tag{3.29}$$

Since

$$\int_0^L \exp(\frac{-j2\pi nl}{L})dl = 0 \quad , \tag{3.30}$$

for $n = 0$

$$c'_0 = \frac{Sexp(j\theta)}{L}\int_0^L u(l)dl + \frac{Sexp(j\theta)}{L}\int_0^L (T_x+jT_y)dl$$

or

$$c'_0 = Sexp(j\theta)[c_0+T_x+jT_y] \tag{3.31}$$

From the above equations it is clear that the ratio $\frac{c'_n}{c_n}$ can be used to estimate the scaling (S) as well as the rotation (θ) parameters. Once S and θ are known, equating the real and imaginary parts of equation (3.31) yield estimates of the translation parameters T_x and T_y respectively.

In practice the impedance plane data is sampled. Persoon and Fu [22] provide a procedure for estimating the Fourier coefficients by approximating the curve by a polygon

of m sides with vertices at $v_0, v_1, \cdots, v_{m-1}$. The vertices correspond to the data points of the impedance plane trajectory. Vertex $v_m = v_0$ to satisfy the assumption of a closed curve. The expression for estimating c_n is as follows:

$$c_n = \frac{L}{4\pi^2 n^2} \sum_{k=1}^{m} (b_{k-1} - b_k) \exp(\frac{-j2\pi n l_k}{L}), \qquad n \neq 0 \tag{3.32}$$

$$c_0 = \frac{1}{m} \sum_{k=1}^{m} v_k \tag{3.33}$$

where

$$l_k = \sum_{i=1}^{k} |v_i - v_{i-1}|, \qquad k > 0 \qquad \text{and} \qquad l_0 = 0 \tag{3.34}$$

and

$$b_k = \frac{v_{k+1} - v_k}{|v_{k+1} - v_k|} \tag{3.35}$$

The estimates of c_n can be used to calculate the scaling and rotation parameters. Although technically, any coefficient pair can be used to calculate these parameters, it is preferable to use coefficients that are large valued. This usually implies the use of lower order coefficients. Coefficients ranging from c_{-10} to c_{10} were calculated and used to estimate S and θ. All of them gave similar values for the parameters. The translation parameters were estimated using c_0. The computational burden of associated with the use of Fourier series based method is significantly lower compared to the time domain conjugate gradient method. The procedure is $O(N)$ where N is the number of samples.

Figure 3.4(a) shows support plate signal obtained at the primary frequency, 3.4(b) shows the auxiliary frequency signal and 3.4(c) shows the original and transformed signals.

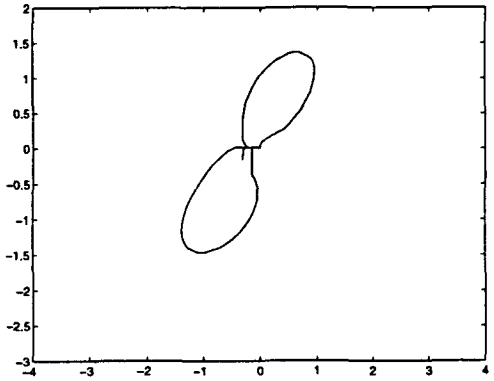

(a) Primary frequency signal at 400kHz

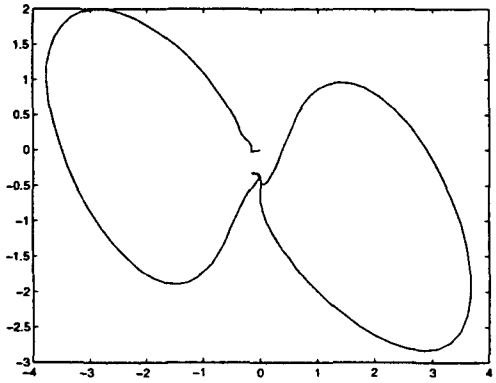

(b) Auxiliary frequency signal at 200kHz

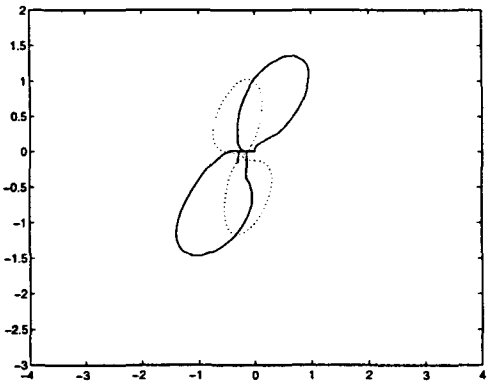

(c) signal in (b) translated to (a)

Figure 3.4 Support plate signal translation using Fourier series method: dotted line shows the transformed signal

It is obvious from the results shown in Figure 3.4 that the procedure is not satisfactory. This is due to the fact that the algorithm assumes

$$S_x = S_y = S$$

The reduction in the degrees of freedom clearly affects the performance. The algorithm is not able to match the FEM impedance plane data pairs that was used for evaluating algorithm using the conjugate gradient method. This is understandable since the optimal values of $S_x = -2.6681$ and $S_y = 1.8923$ are different. It must be mentioned though that the frequency domain methods are not iterative and involve a fixed amount of computation, which is a significant advantage relative to the time domain methods. This limitation led to the search for other frequency domain methods which would allow independent scaling of the inphase and quadrature components of the impedance plane data. One such method that was investigated uses the cosine transform for obtaining the frequency domain representation.

3.5 Discrete cosine transform method

The discrete cosine transform (DCT) of a data sequence,

$X(m), \quad m = 0, 1, \cdots, (n-1)$ is defined as

$$G_x(0) = \frac{\sqrt{2}}{n} \sum_{m=0}^{n-1} X(m) \tag{3.36}$$

$$G_x(k) = \frac{2}{n} \sum_{m=0}^{n-1} X(m) \cos \frac{(2m+1)k\pi}{2n}, \qquad k = 1, 2, ..., (n-1) \tag{3.37}$$

where $G_x(k)$ is the k^{th} DCT coefficient.

As can be seen, the DCT is a real transform [9]. This means that the DCT can be evaluated for expanding the inphase and the quadrature components of the impedance plane data independent of each other.

Let S_a and S_b be the sequences as defined earlier. The sequence S_a is given by

$$(x_0, y_0), (x_1, y_1), (x_2, y_2) \cdots, (x_{n-1}, y_{n-1})$$

where n is the length of the sequence

The points represent complex impedance of the probe coil in the complex impedance plane. Hence the sequence may also be written as

$$(x_0 + jy_0), (x_1 + jy_1), \cdots, (x_{n-1} + jy_{n-1})$$

Also the sequence $Re(S_a)$ is the real part of sequence S_a given by

$$x_0, x_1, x_2 \cdots, x_{n-1}$$

Similarly the sequence $Im(S_a)$ is the imaginary part of the sequence and is given by

$$y_0, y_1, y_2 \cdots, y_{n-1}$$

The sequence S'_a is the transformed signal so that it maps to the basic frequency signal S_b.

The sequence S'_a is given by

$$(x'_0, y'_0), (x'_1, y'_1), (x'_2, y'_2), \cdots, (x'_{n-1}, y'_{n-1})$$

The sequence S'_a is obtained using the transformation

$$S'_a = S_a \mathbf{A}(T_x, T_y, \theta, S_x, S_y)$$

where the matrix $\mathbf{A}$ is given by:

$$\mathbf{A} = \begin{bmatrix} S_x \cos\theta & S_y \sin\theta \\ -S_x \sin\theta & S_y \cos\theta \\ S_x(T_x \cos\theta - T_y \sin\theta) & S_y(T_x \sin\theta + T_y \cos\theta \end{bmatrix}$$

Alternatively the relation between the sequences S_a and S'_a can be written as:

$$[x', y'] = [x, y, 1]A$$

The above affine transform relation between data sequences S_a and S'_a in the expanded form is given by:

$$\begin{aligned} x' &= xS_x \cos\theta - yS_x \sin\theta + S_x(T_x \cos\theta - T_y \sin\theta) \\ &= xS_x \cos\theta - yS_x \sin\theta + a_{31} \qquad (3.38) \\ y' &= xS_y \sin\theta + yS_y \cos\theta + S_y(T_x \sin\theta + T_y \cos\theta) \\ &= xS_y \sin\theta + yS_y \cos\theta + a_{32} \qquad (3.39) \end{aligned}$$

where

a_{31} and a_{32} represent appropriate elements of the matrix **A**.

The DCT of $Re(S_a)$ denoted by G_x is

$$G_x(0) = \frac{\sqrt{2}}{n} \sum_{m=0}^{n-1} x_m \qquad (3.40)$$

$$G_x(k) = \frac{2}{n} \sum_{m=0}^{n-1} x_m \cos\frac{(2m+1)k\pi}{2n}, \qquad k = 1, 2, ..., (n-1) \qquad (3.41)$$

The DCT of $Re(S'_a)$ denoted by G'_x is

$$G'_x(0) = \frac{\sqrt{2}}{n} \sum_{m=0}^{n-1} x'_m \qquad (3.42)$$

$$G'_x(k) = \frac{2}{n} \sum_{m=0}^{n-1} x'_m \cos\frac{(2m+1)k\pi}{2n}, \qquad k = 1, 2, ..., (n-1) \qquad (3.43)$$

Substituting for x'_m in the above relation using equation (3.37) gives,

$$\begin{aligned} G'_x(0) &= \frac{\sqrt{2}}{n} \sum_{m=0}^{n-1} (x_m S_x \cos\theta - y_m S_x \sin\theta + a_{31}) \\ &= \frac{\sqrt{2}}{n} \sum_{m=0}^{n-1} (x_m S_x \cos\theta) - \frac{\sqrt{2}}{n} \sum_{m=0}^{n-1} (y_m S_x \sin\theta) + \frac{\sqrt{2}}{n} \sum_{m=0}^{n-1} a_{31} \end{aligned}$$

$$= S_x \cos\theta \frac{\sqrt{2}}{n} \sum_{m=0}^{n-1} x_m - S_x \sin\theta \frac{\sqrt{2}}{n} \sum_{m=0}^{n-1} y_m + \frac{\sqrt{2}}{n} \sum_{m=0}^{n-1} a_{31}$$

$$= S_x \cos\theta G_x(0) - S_x \sin\theta G_y(0) + a_{31}\sqrt{2} \tag{3.44}$$

Similarly,

$$\begin{aligned} G'_x(k) &= \frac{2}{n} \sum_{m=0}^{n-1} x'_m \cos\frac{(2m+1)k\pi}{2n} \\ &= \frac{2}{n} \sum_{m=0}^{n-1} (x_m S_x \cos\theta - y_m S_x \sin\theta + a_{31}) \cos\frac{(2m+1)k\pi}{2n} \\ &= S_x \cos\theta \frac{2}{n} \sum_{m=0}^{n-1} x_m \cos\frac{(2m+1)k\pi}{2n} \\ &- S_x \sin\theta \frac{2}{n} \sum_{m=0}^{n-1} y_m \cos\frac{(2m+1)k\pi}{2n} \\ &+ a_{13} \frac{2}{n} \sum_{m=0}^{n-1} \cos\frac{(2m+1)k\pi}{2n} \\ &= S_x \cos\theta G_x(k) - S_x \sin\theta G_y(k) \end{aligned} \tag{3.45}$$

The constant term in $G'_x(k)$ vanishes since

$$\frac{2}{n} \sum_{m=0}^{n-1} \cos\frac{(2m+1)k\pi}{2n} = 0, \qquad k = 1, 2, \cdots, (n-1) \tag{3.46}$$

Similar computations for $G'_y(0)$ and $G'_y(k)$ give the following relations

$$G'_y(0) = S_y \sin\theta G_x(0) + S_y \cos\theta G_y(0) + a_{32}\sqrt{2} \tag{3.47}$$

$$G'_y(k) = S_y \sin\theta G_x(k) + S_y \cos\theta G_y(k) \tag{3.48}$$

For $k = 1, 2, \cdots, (n-1)$, the above relations can also be written as

$$G'_x(k) = S_x Re[G(k)e^{j\theta}] \tag{3.49}$$

$$G'_y(k) = S_y Im[G(k)e^{j\theta}] \tag{3.50}$$

where

$G(k) = G_x(k) + jG_y(k)$

The above equations clearly show the relation between the DCT coefficients of sequences S_a and S'_a. Given the DCT coefficients of sequences S_a and S_b, it is possible using the above equations to calculate the values of the translation parameters. The advantage over the Fourier series method described earlier is that the equations allow determination of the parameters S_x and S_y. Another advantage of the DCT is that fast FFT based algorithms can be used to calculate the DCT coefficients. This has major implications with regard to the computational burden associated with these algorithms.

The affine transform parameters $T_x, T_y, \theta, S_x, S_y$ can be calculated as follows.

Let

$$R_{k_1 k_2} = \frac{G'_x(k_1)}{G'_x(k_2)} \tag{3.51}$$

Hence

$$R_{k_1 k_2} = \frac{G'_x(k_1)}{G'_x(k_2)} = \frac{Re[G(k_1)e^{j\theta}]}{Re[G(k_2)e^{j\theta}]} \tag{3.52}$$

Expanding the above equation and rearranging the terms gives:

$$\tan\theta = \frac{R_{k_1 K_2} G_x(k_2) - G_x(k_1)}{R_{k_1 K_2} G_y(k_2) - G_y(k_1)} \tag{3.53}$$

This gives two values of θ between $0 - 360$ which are 180 degrees apart (say θ_1 and $\theta_1 + \pi$)

After θ is estimated, S_x can be calculated using

$$S_x = \frac{G'_x(k_1)}{Re[G(k_1)e^{j\theta}]} \tag{3.54}$$

Similarly,

$$S_y = \frac{G'_y(k_1)}{Im[G(k_1)e^{j\theta}]} \tag{3.55}$$

$$\tag{3.56}$$

As can be verified from the equations (3.54) and (3.55) if the solution using θ_1 is S_{x1} and S_{y1} the other solution obtained using $\theta = \theta_1 + \pi$ is, $-S_{x1}$ and $-S_{y1}$. The two solutions result in same values for the parameters T_x and T_y. Both sets of solutions map the auxiliary frequency signal to the primary frequency signal in an identical manner. This can also be verified by replacing θ in the matrix A with $\theta+\pi$ and S_x, S_y by $-S_x, -S_y$ respectively.

T_x and T_y are calculated from equations (3.43) and (3.46) relating the zeroth DCT coefficients of the two signals. All other terms in the equations are known, consequently the two equations can be solved simultaneously for T_x and T_y.

The algorithm for finding the optimal affine transform parameters is implemented using the above equations. The DCT coefficients are calculated for the primary and the auxiliary frequency signals. These coefficients can be evaluated efficiently using fast algorithms [1] [20]. Another noteworthy aspect of this procedure is that only the first few DCT coefficients need to be calculated. This reduces the computational burden even further. Once the DCT coefficients are calculated, the optimal transform parameters can be estimated using the above equations.

It can be seen that the parameters can be estimated using any arbitrary value of k_1 and k_2. However it has been observed, that not all coefficients provide identical estimates of the parameters. Hence the optimal parameters are those that result in a minimum value for the cost function E. Figure 3.5 shows the results obtained using the DCT based algorithm for calculating the optimal affine transform parameters for the FEM modeled data. The results are the same as those obtained using the conjugate gradient method. Additional results are presented in the next chapter.

The closed form relations between the DCT coefficients of the primary and auxiliary frequency signals suggests that invariant feature vectors can be found which would be insensitive to translation, rotation and scaling of the original signal. These invariant features are dependent only on the shape of the impedance plane trajectory. This result

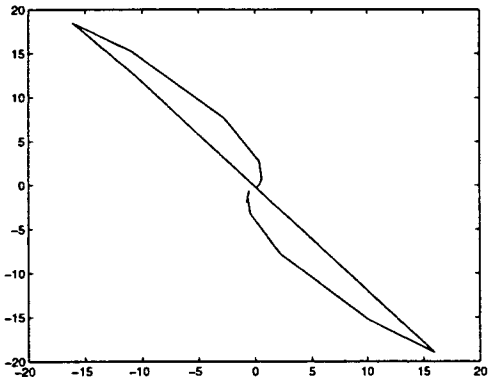

(a) Primary frequency signal at 50kHz

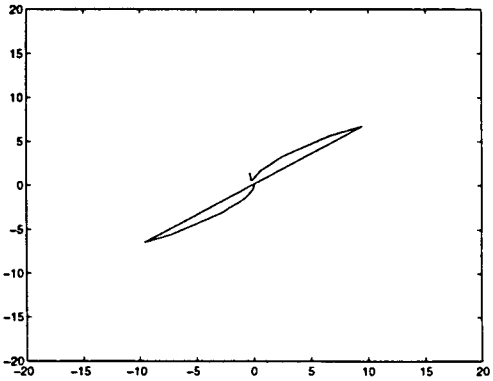

(b) Auxiliary frequency signal at 25kHz

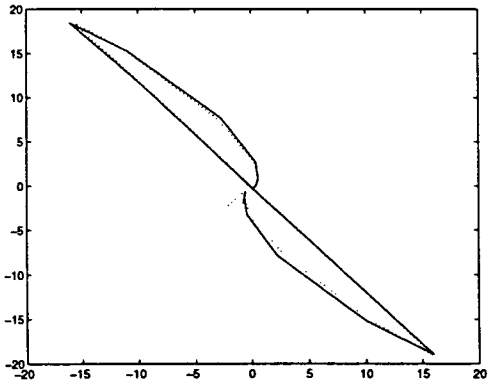

(c) signal in (b) translated to (a)

Figure 3.5 Signal transformation for FEM generated data using DCT coefficients

is of great significance especially in the area of NDT since the invariant descriptors can be embedded in feature vectors for the classification of defect signals. This is an important outcome of the above analysis and is presented next.

3.5.1 Invariant parameters using DCT

The DCT terms vary if the signal is rotated, scaled and translated. In order to obtain descriptors that are invariant to these transformations, we begin by defining the function,

$$A(k_1, k_2, k_3, k_4) = \frac{G_x(k_1)G_y(k_2) - G_y(k_1)G_x(k_2)}{G_x(k_3)G_y(k_4) - G_y(k_3)G_x(k_4)} \tag{3.57}$$

It can be shown that $A(k_1, k_2, k_3, k_4)$ is invariant to these transformations. This can be proved as follows:

Define $B(k_1, k_2) = G_x(k_1)G_y(k_2) - G_y(k_1)G_x(k_2)$

Hence

$$A(k_1, k_2, k_3, k_4) = \frac{B(k_1, k_2)}{B(k_3, k_4)} \tag{3.58}$$

Now

$$\begin{aligned}
B'(k_1, k_2) &= G'_x(k_1)G'_y(k_2) - G'_y(k_1)G'_x(k_2) \\
&= S_x S_y[(G_x(k_1)\cos\theta - G_y(k_1)\sin\theta)(G_x(k_2)\sin\theta + G_y(k_2)\cos\theta) \\
&- (G_x(k_2)\cos\theta - G_y(k_2)\sin\theta)(G_x(k_1)\sin\theta + G_y(k_1)\cos\theta)] \\
&= S_x S_y[G_x(k_1)\cos\theta G_x(k_2)\sin\theta + G_x(k_1)\cos\theta G_y(k_2)\cos\theta \\
&- G_y(k_1)\sin\theta G_x(k_2)\sin\theta - G_y(k_1)\sin\theta G_y(k_2)\cos\theta \\
&- G_x(k_2)\cos\theta G_x(k_1)\sin\theta - G_x(k_2)\cos\theta G_y(k_1)\cos\theta \\
&+ G_y(k_2)\sin\theta G_x(k_1)\sin\theta + G_y(k_2)\sin\theta G_y(k_1)\cos\theta]
\end{aligned}$$

which on rearranging gives

$$= S_x S_y[G_x(k_1)G_y(k_2) - G_y(k_1)G_x(k_2)]$$

$$= S_x S_y B(k_1, k_2) \tag{3.59}$$

Consequently,

$$\begin{aligned} A'(k_1, k_2, k_3, k_4) &= \frac{B'(k_1, k_2)}{B'(k_3, k_4)} \\ &= \frac{S_x S_y B(k_1, k_2)}{S_x S_y B(k_3, k_4)} \\ &= A(k_1, k_2, k_3, k_4) \end{aligned} \tag{3.60}$$

Hence the function defined by $A(k_1, k_2, k_3, k_4)$ is invariant under rotation, independent scaling of the X and Y components, and translation along the X and Y axis. The above function defines a family of invariant features. By experimenting with various combinations of the coefficient k_1, k_2, k_3 and k_4, appropriate feature vectors can be constructed and used for training a neural network for defect classification.

Figure 3.6 plots the function $A(k_1, k_2, k_3, k_4)$ for the FEM derived primary frequency data and the same data after being translated, scaled and rotated by arbitrarily chosen amount. The dotted lines show the invariant features for the primary frequency signal and the points marked by 'x' shows for the translated signal. The index along the X axis stands for k_1. The variables k_2, k_3 and k_4 are set equal to $k_1 + 1$, $k_1 + 2$ and $k_1 + 3$ respectively. As can be seen the feature vectors match perfectly for the FEM modeled primary frequency impedance plane trajectory and its transformed version.

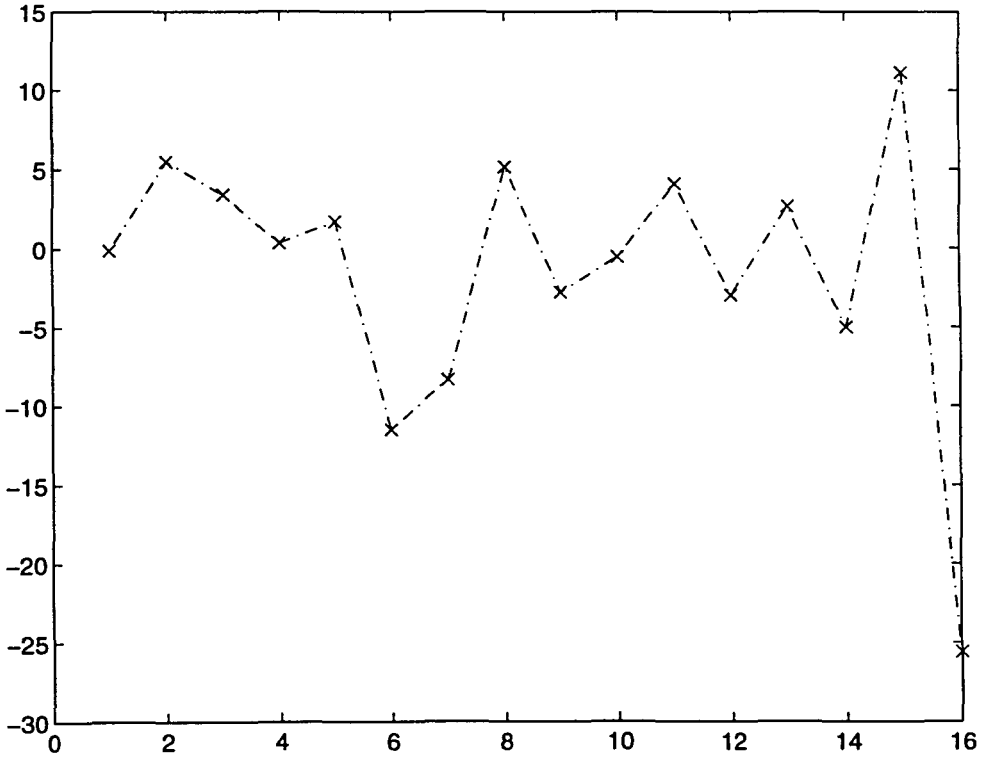

Figure 3.6 Invariant features for FEM modeled signal

4 RESULTS AND CONCLUSIONS

The multifrequency eddy current analysis techniques developed in the previous chapters are evaluated using experimental data. The results obtained using the new methods were compared with those obtained using a commercial eddy current multifrequency instrument (MIZ-40, Zetec Inc.) The MIZ-40 was used for collecting eddy current defect signatures at multiple excitation frequencies in the presence of a support plate.

The experimental setup consisted of a calibration tube with machined defects such as through-wall hole defect, deep flat bottom holes, 60%, 40% and 20% wall thickness deep and 2 mm wide OD defects. A ferromagnetic support ring was used to simulate a support plate. A differential eddy current probe excited simultaneously at two different frequencies is used to the collect eddy current signals. Data obtained at two frequencies are normally sufficient to nullify the effect of a support plate. The primary and auxiliary excitation frequencies are selected experimentally by following the procedure outlined in chapter 2. It was observed that using a primary frequency of 400 kHz and an auxiliary frequency of 200 kHz achieves the best phase and amplitude separation between the defect and the unwanted support plate signal, for the given setup. The complex impedance of the differential probe is displayed on the instrument for each excitation frequency, after separating the test frequencies and digitizing the signal. A sampling rate of 400 Hz is used for digitization which is considered sufficient. A multiplexed version of the eddy current signals, is available through the analog output ports of the instrument. These signals are sampled at 1 kHz but since the signal is multiplexed, the effective sampling rate for each frequency is 100 Hz. This is the signal that is used

for multiparameter analysis using the approaches that have been developed. Since the maximum sampling rate available is 100 Hz, the sampling rate on MIZ-40 is also set to the same value for comparison.

Figure 4.1 presents the step by step method used by MIZ-40 for support plate suppression. First, the support ring is placed on a defect free region of the tube. The tube is scanned and pure support plate signatures are obtained. These are displayed in Figure 4.1(a) and 4.1(c). The mixing parameters are calculated from these signals and stored. The tube is scanned again, this time to locate and characterize flaws in the tube. As the tube is scanned, the auxiliary excitation frequency data are transformed using the mixing parameters, subtracted from the basic frequency data, and then displayed on the instrument screen. Figure 4.1 shows the results obtained using this approach on data collected from the instrument. The affine transform based conjugate gradient method was used to calculate the transformation parameters T_x, T_y, θ, S_x and S_y. Figure 4.1(e) shows the auxiliary support signal (dotted lines) translated to map the primary frequency support signal which is also displayed. The result of subtraction is shown in Figure 4.1(g). As can be observed, the residual signal after subtraction is small. Figure 4.1(b) and Figure 4.1(d) show the composite signal when the support ring is placed above the through-hole defect. Figure 4.1(f) shows the auxiliary frequency composite signal mapped onto the primary frequency composite signal using the transformation parameters calculated above. Figure 4.1(h) shows the final result of subtraction of the translated composite signal from the primary composite signal. The support plate signal is completely suppressed (except for the residue in the center which does not affect the phase analysis). Figure 4.2 shows the same steps for the MIZ-40 instrument. The algorithm used by MIZ-40 for calculating the transformation parameters is not known. A comparison of Figure 4.1(h) and 4.2(f) shows that similar results are obtained for MIZ-40 and the time-domain conjugate gradient method. Figure 4.3 presents the results obtained from the Zetec instrument and the conjugate gradient method for comparison,

for a 60 % wall thickness and 2 mm wide OD defect with the support ring aligned with the defect. The poor quality of the defect signal is a direct consequence of the low sampling rate. This is clear from 4.3(g) which shows the defect signal after support plate suppression (done on MIZ-40) at 400 Hz sampling rate.

The method used by MIZ 40 for support plate suppression is not very efficient since in reality the nature of the support plate signal may be different from the artifact standard that is used during the calibration stage. It is also likely to be different for support plates located along the tubes due to the varying conditions that exist in nuclear power plants. The alternative approach that is proposed in this thesis uses the composite signals for calculating the transformation parameters. The parameters are used to translate the auxiliary frequency signal to the primary signal which is then subtracted from the primary frequency signal to nullify the effect of the support plate. Similar results are obtained using the same approach for a through-hole defect as shown in Figure 4.4. The conjugate gradient based approach is used for calculating the translation parameters.

The results obtained using cosine transform based method are similar to the results obtained using the time-domain conjugate gradient method. This is demonstrated in Figure 4.5 for the through-wall hole defect. The results are compared with those obtained using the MIZ-40 instrument for a 40 % OD defect in Figure 4.6. The cosine transform based method was used to estimate the translation parameters from the composite signal in this case. In effect, the results obtained using the conjugate gradient and the cosine transform based techniques are similar to those obtained using the MIZ-40 instrument both when the support plate signal in the defect free region is used for mixing or when the composite signals are directly mixed.

4.1 Conclusions and recommendations for future work

A novel approach for eddy current signal analysis has been described in this thesis. The validity of the approach has been demonstrated using experimental data. The theoretical basis for the cosine transform based approach is presented in chapter 3. The time domain approach provides an optimal result as it minimizes a cost function in the least squares error sense. The cosine transform based approach achieves similar results with the additional benefit that it involves a fixed computational effort. The computational effort associated with the conjugate gradient method is variable. A comparison of the results shows that the proposed approaches offer performance levels that are similar to those using MIZ-40. The DCT based method is superior to the Fourier series method. However the proposed techniques are computationally fast and can be implemented in real time. The proposed methods also do not require the mixing to be optimized for each extraneous discontinuity that is encountered as the tube is inspected. Additionally the new methods do not require the user to undergo a calibration procedure.

These techniques will be incorporated in the multifrequency eddy current instrument that is being developed by the MCRG group at Iowa State University. The function $A(k_1, k_2, k_3, k_4)$ described in chapter 3 defines a family of invariant features that are independent of scaling, rotation and translation of the signal. A more detailed study of these invariant features should be conducted so that appropriate features can be selected and used for defect signal classification in automated NDE systems. An alternate Fourier series based approach can be investigated by encapsulating the real and imaginary components of the impedance in a two dimensional vector of real and imaginary components. This might allow independent scaling of the real and imaginary components of the impedance plane data, so that the signals can be mapped more accurately. The method does not work for all pairs of DCT coefficients. This needs further investigation.

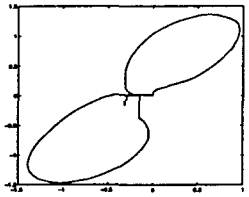

(a) Support plate (400kHz)

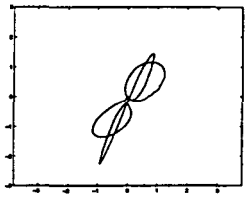

(b) Support plate and defect (400kHz)

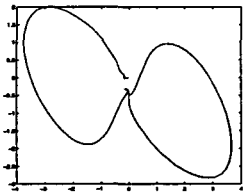

(c) Support (200kHz)

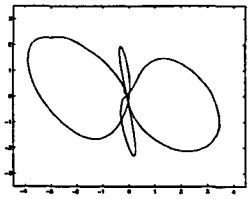

(d) Support and defect (200kHz)

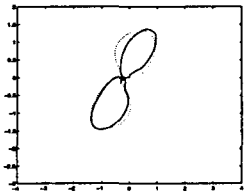

(e) transformed support signal

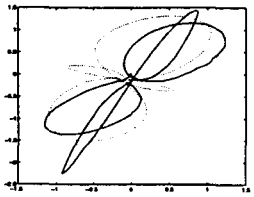

(f)transformed defect signal

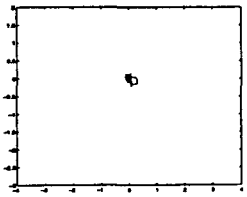

(g) mixed support signal

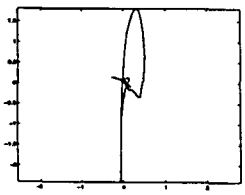

(h)mixed defect signal

Figure 4.1 Mixing results using conjugate gradient technique for a through hole defect in the presence of a support plate

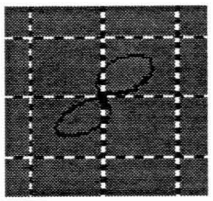

(a) Support plate (400kHz)

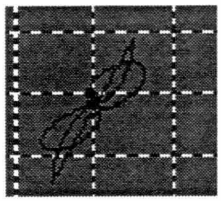

(b) Support plate and defect (400kHz)

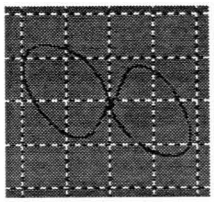

(c) Support (200kHz)

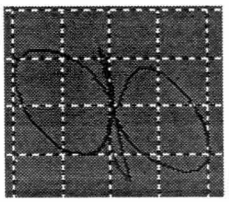

(d) Support and defect (200kHz)

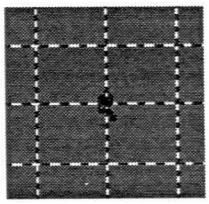

(e) mixed support signal

(f)mixed defect signal

Figure 4.2 Mixing results for MIZ-40 instrument for a through hole defect in the presence of a support plate

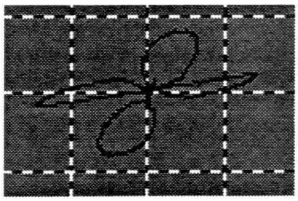

(a) Primary frequency signal

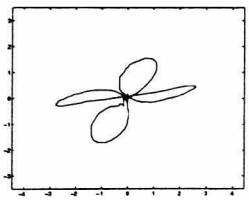

(b) Primary frequency signal

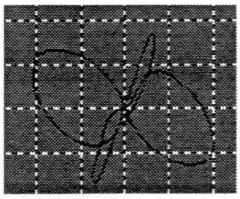

(c) Auxiliary frequency signal

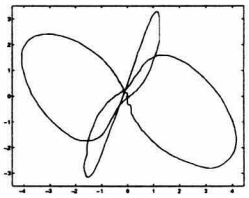

(d) Auxiliary frequency signal

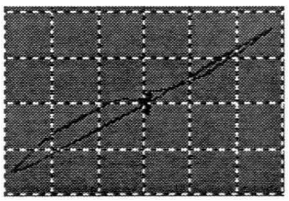

(e) Zetec Mix

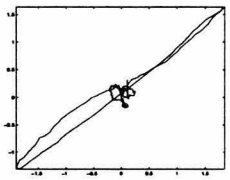

(f) Mix using affine transform

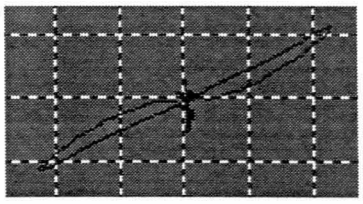

(g) Zetec Mix, 400 Hz sampling rate

Figure 4.3 60% OD defect in the presence of support plate: a,c,e are obtained using the MIZ-40 instrument, b,d,f are obtained using the conjugate gradient technique

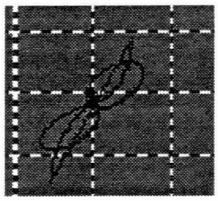

(a) Primary frequency signal

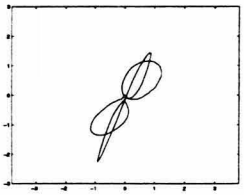

(b) Primary frequency signal

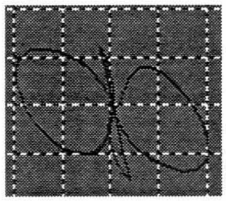

(c) Auxiliary frequency signal

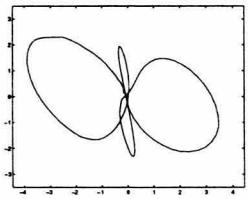

(d) Auxiliary frequency signal

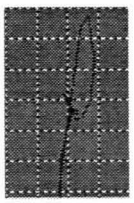

(e) Zetec Mix

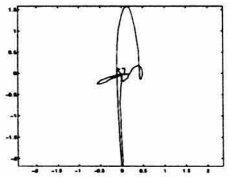

(f) Mix using affine transform

Figure 4.4 Through hole defect in the presence of support plate: a,c,e are obtained using the MIZ-40 instrument, b,d,f are obtained using the conjugate gradient method on the composite signal

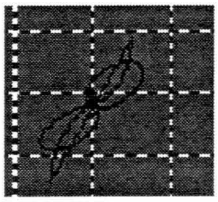

(a) Primary frequency signal

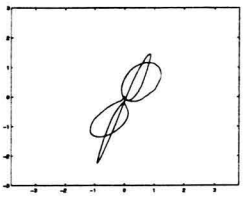

(b) Primary frequency signal

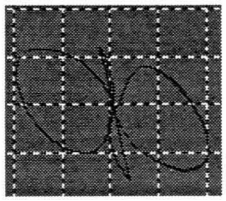

(c) Auxiliary frequency signal

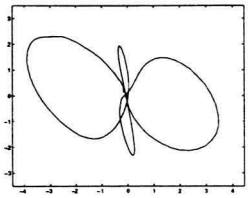

(d) Auxiliary frequency signal

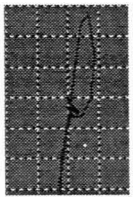

(e) Zetec Mix

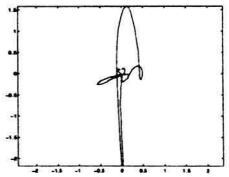

(f) Mix using cosine transform approach

Figure 4.5 Through hole defect in the presence of support plate: a,c,e are obtained using the MIZ-40 instrument, b,d,f are obtained using the cosine transform based approach on the composite signal

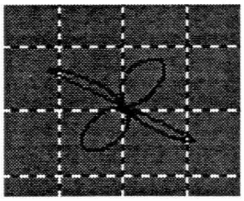

(a) Primary frequency signal

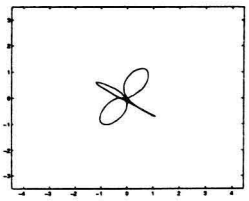

(b) Primary frequency signal

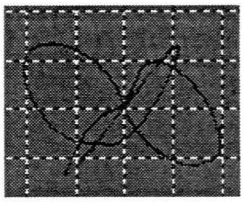

(c) Auxiliary frequency signal

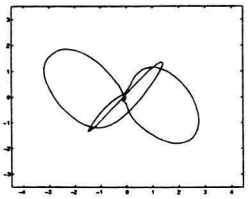

(d) Auxiliary frequency signal

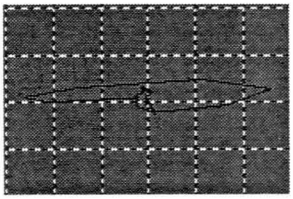

(e) Zetec Mix

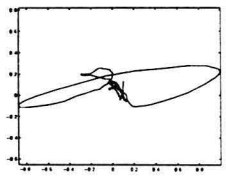

(f) Mix using affine transform

Figure 4.6 40% OD defect in the presence of support plate: a,c,e are obtained using the MIZ-40 instrument, b,d,f are obtained using the cosine transform based approach on the composite signal

BIBLIOGRAPHY

[1] N. Ahmed, T. Natarajan, and K.R. Rao, "Discrete cosine transform," *IEEE transactions on computers*, Jan. 1994, pp. 90-93.

[2] K.J. Bowker, M.C. Warnes and M.D. Ashworth, "Some developments in eddy current techniques for in-service inspection," *Insight* Vol. 37, No. 3, March 1995. pp. 163-168.

[3] S.D. Brown, "Multifrequency/Multiparameter eddy current steam generator NDE," *Quantitative NDE in the nuclear industry*, Edited by R.B. Clough, American Society For Metals, Metals Park, Ohio, 1983. pp 99-105.

[4] "Field experiences with multifrequency-multiparameter eddy current technology," EPRI NP-2299. Batelle, Columbus Laboratories and EPRI NDE Center. Electric Power Research Institute, Palo Alto, Calofornia March 1982.

[5] R.K. Granville, "In service eddy current examination of non-ferrous industrial heat exchanger tubing," *British journal of NDT*, Vol. 33, No. 8, Aug. 1991, pp. 403-408

[6] D.J. Hagemaier, *Fundamentals of eddy current testing*, American Society for Nondestructive Testing, Columbus, Ohio, 1990.

[7] "Eddy current inspection of non-ferrous heat-exchanger tubing," *Insight*, Vol. 36, No. 4, April 1994, pp. 218-220.

[8] D. Horne, S. Udpa and W. Lord, "Superposition of eddy current probe signals," *Materials Evaluation*, Vol. 42, June 1984, pp. 930-933.

[9] A.K. Jain, *Fundamentals of digital image processing*, Prentice hall of Private limited, New Delhi, 1995. pp. 150-154.

[10] M. Junger, C. Brook, "Beginner's guide to sensor selection and evaluation techniques for eddy current testing," *British journal of NDT*, Vol. 32, No. 9, Sept. 1990, pp. 463-466.

[11] D. Kahaner, C. Moler and S. Nash, *Numerical methods and software*, Englewood Cliffs, Prentice-Hall, New Jersey, 1989.

[12] H.L. Libby, "Eddy current test for tubing flaws in support regions," *Research techniques in nondestructive testing*, Vol. 2 Edited by R.S. Sharpe, London, Academic Press,1973, pp. 151-184.

[13] H.L. Libby, *Introduction to electromagnetic nondestructive test methods*, John Wiley & Sons, New York, 1971.

[14] *Electromagnetic methods of nondestructive testing*, Edited by W. Lord, Gordon and Breach Science Publishers, London, 1985, pp. 175-304.

[15] R.C. McMaster, *Nondestructive testing handbook*, Vol. 1, American Society for Nondestructive Testing, Columbus, Ohio, 1959.

[16] R.C. McMaster, *Nondestructive testing handbook*, Vol. 2, American Society for Nondestructive Testing, Columbus, Ohio, 1959.

[17] R.C. McMaster, P. McIntire and M.L. Mester, *Nondestructive testing handbook*, Vol. 4, 2^{nd} ed., American Society for Nondestructive Testing, Columbus, Ohio, 1986.

[18] R.C. McMaster, "The present and future of eddy current testing," *Materials Evaluation* , Vol. 43, Nov. 1985, pp. 1512-1521.

[19] J.A. Mundis and G.W. DeYoung, "Solutions to NDE problems in PWR steam generators-an overview," *Quantitative NDE in the nuclear industry*, Edited by R.B. Clough, American Society for Metals, Metals Park, Ohio, 1983, pp. 93-98.

[20] M.J. Narasimha, A.M. Peterson, "On the computation of the discrete cosine transform," *IEEE transactions on communications*, Vol. COM-26, No. 6, June 1978, pp. 934-936.

[21] R. Palanisamy and W. Lord, "Finite element analysis of eddy current phenomena," *Materials Evaluation*, Vol. 38, No. 10, Oct. 1980, pp. 39-43.

[22] E. Persoon, and K.S. Fu, "Shape discrimination using Fourier descriptors," *IEEE transactions on systems, man and cybernetics*, Vol. SMC-7, No. 3, March 1977.

[23] L. de la Pintiere, "Back to basics," *Materials Evaluation*, Vol. 43, Feb. 1985, pp. 152-153.

[24] J.M. Prince, L.D. Reid, D.L. Lessor, "Two-frequency eddy current instrument for measuring the thickness of Zircaloy cladding on Uranium under conditions of varying lift-off," *Materials Evaluation*, Vol. 43, Nov. 1985, pp. 1562-1565.

[25] S.S. Rao, "Nonlinear programming II: Unconstrained optimization techniques," chapter 6, *Optimization theory and applications*, Wiley Eastern Limited, New Delhi, India, 1978.

[26] R. Saglio and M. Pigeon, "Concepts of multifrequency eddy current testing", *Electromagnetic testing*, Vol. 4, 2^{nd} Ed., Edited by P. McIntire, R. McMuster, American Society for Nondestructive testing, Columbus, Ohio, 1986, pp. 592-605.